DUDLEY KNOX LIBRARY
NAVAL POSTGRADUATE SCHOOL
MONTEREY, CALIFORNIA 93943-5002

NAVAL POSTGRADUATE SCHOOL
Monterey, California

THESIS

A THEORETICAL EXAMINATION
OF A RE-ENTRY CAPSULE
INCORPORATING AN AUTOROTATING ROTOR

by

Robert G. Struth, Jr.

December 1986

Thesis Advisor: Donald M. Layton

Approved for public release; distribution is unlimited.

T233067

SECURITY CLASSIFICATION OF THIS PAGE

REPORT DOCUMENTATION PAGE

1a REPORT SECURITY CLASSIFICATION UNCLASSIFIED	1b RESTRICTIVE MARKINGS
2a SECURITY CLASSIFICATION AUTHORITY	3 DISTRIBUTION / AVAILABILITY OF REPORT Approved for public release; distribution is unlimited.
2b DECLASSIFICATION / DOWNGRADING SCHEDULE	
4 PERFORMING ORGANIZATION REPORT NUMBER(S)	5 MONITORING ORGANIZATION REPORT NUMBER(S)
6a NAME OF PERFORMING ORGANIZATION Naval Postgraduate School 6b OFFICE SYMBOL (If applicable) 31	7a NAME OF MONITORING ORGANIZATION Naval Postgraduate School
6c ADDRESS (City, State, and ZIP Code) Monterey, CA 93943-5000	7b ADDRESS (City, State, and ZIP Code) Monterey, CA 93943-5000
8a NAME OF FUNDING / SPONSORING ORGANIZATION 8b OFFICE SYMBOL (If applicable)	9 PROCUREMENT INSTRUMENT IDENTIFICATION NUMBER
8c ADDRESS (City, State, and ZIP Code)	10 SOURCE OF FUNDING NUMBERS PROGRAM ELEMENT NO / PROJECT NO / TASK NO / WORK UNIT ACCESSION NO

11 TITLE (Include Security Classification)

A THEORETICAL EXAMINATION OF A RE-ENTRY CAPSULE INCORPORATING AN AUTOROTATING ROTOR

12 PERSONAL AUTHOR(S)
Struth, Robert G., Jr.

13a TYPE OF REPORT	13b TIME COVERED	14 DATE OF REPORT (Year Month Day)	15 PAGE COUNT
Master's Thesis	FROM ____ TO ____	1986 December	72

16 SUPPLEMENTARY NOTATION

17 COSATI CODES			18 SUBJECT TERMS (Continue on reverse if necessary and identify by block number)
FIELD	GROUP	SUB-GROUP	Rotor re-entry vehicle, rotor entry vehicle, lifting re-entry, lifting rotor, rotor aerodynamics, aerodynamic heat transfer, performance, rotary wings, drag

19 ABSTRACT (Continue on reverse if necessary and identify by block number)

A theoretical analysis was conducted to determine the aerodynamic and performance characteristics of a capsule incorporating an autorotating rotor for recovery from earth orbit. The potential advantages of this combination include the reduction of landing speeds to improve the chances of successful emergency landings on water, uneven terrain, or during inclement weather. Since others have concentrated on the approach and landing phases, the aim herein was to determine the range, deceleration, and heating effects during the entire re-entry. Rotor-to-capsule diameter and rotor deployment time were varied along with type of recovery, i.e., capsule lifting or nonlifting. The addition of a rotor was found to provide a significant increase in lateral range capability while changing maximum deceleration only slightly; however, excessive aerodynamic rotor heating requires either delayed deployment (reducing the performance gains) or substitution/development of structural materials having higher heat resistance than those studied.

20 DISTRIBUTION / AVAILABILITY OF ABSTRACT	21 ABSTRACT SECURITY CLASSIFICATION
☒ UNCLASSIFIED/UNLIMITED ☐ SAME AS RPT ☐ DTIC USERS	UNCLASSIFIED
22a NAME OF RESPONSIBLE INDIVIDUAL Donald M. Layton	22b TELEPHONE (Include Area Code) (408) 646-2997 22c OFFICE SYMBOL 67Ln

DD FORM 1473, 84 MAR 83 APR edition may be used until exhausted
All other editions are obsolete

SECURITY CLASSIFICATION OF THIS PAGE

Approved for public release; distribution is unlimited.

A Theoretical Examination of a Re-entry Capsule Incorporating an Autorotating Rotor

by

Robert G. Struth, Jr.
Lieutenant Commander, United States Navy
B.S., Massachusetts Institute of Technology, 1976
M.S., University of Southern California, 1984

Submitted in partial fulfillment of the
requirements for the degrees of

MASTER OF SCIENCE IN AERONAUTICAL ENGINEERING
and
AERONAUTICAL ENGINEER

from the

NAVAL POSTGRADUATE SCHOOL
December 1986

ABSTRACT

A theoretical analysis was conducted to determine the aerodynamic and performance characteristics of a capsule incorporating an autorotating rotor for recovery from earth orbit. The potential advantages of this combination include the reduction of landing speeds to improve the chances of successful emergency landings on water, uneven terrain, or during inclement weather. Since others have concentrated on the approach and landing phases, the aim herein was to determine the range, deceleration, and heating effects during the entire re-entry. Rotor-to-capsule diameter and rotor deployment time were varied along with type of recovery, i.e., capsule lifting or nonlifting. The addition of a rotor was found to provide a significant increase in lateral range capability while changing maximum deceleration only slightly; however, excessive aerodynamic rotor heating requires either delayed deployment (reducing the performance gains) or substitution/development of structural materials having higher heat resistance than those studied.

TABLE OF CONTENTS

I. INTRODUCTION ---------- 14

A. GENERAL ---------- 14

B. SPECIFIC ---------- 16

C. PRINCIPLES OF OPERATION ---------- 18

1. Axial Descent ---------- 18

2. Glide Flight ---------- 19

3. Touchdown ---------- 19

II. THEORY ---------- 22

A. INTRODUCTION ---------- 22

B. DERIVATION OF OPERATING CHARACTERISTICS -------- 26

C. DERIVATION OF AERODYNAMIC PERFORMANCE CHARACTERISTICS ---------- 28

D. THEORETICAL SOLUTION FOR AXIAL FLOW ---------- 30

E. VEHICLE PERFORMANCE CHARACTERISTICS ---------- 31

1. Aerodynamic Characteristics ---------- 31

2. Atmospheric Re-entry Performance ---------- 31

III. RESULTS AND DISCUSSION ---------- 33

A. INTRODUCTION ---------- 33

B. ROTOR OPERATING CHARACTERISTICS ---------- 33

C. ROTOR AERODYNAMIC CHARACTERISTICS ---------- 35

D. VEHICLE RE-ENTRY PERFORMANCE CHARACTERISTICS --- 36

1. Introduction ---------- 36

2. Range ---------- 40

3. Deceleration ---------- 42

4. Heating ---------- 42

5. Effects of Diameter Ratio on Range, Deceleration, and Heating ---------- 46

6. Effects of Delayed Rotor Deployment -------- 56

IV. CONCLUSIONS ---------- 64

V. RECOMMENDATIONS ---------- 66

A. GENERAL ---------- 66

B. SPECIFIC ---------- 68

LIST OF REFERENCES ---------- 69

INITIAL DISTRIBUTION LIST ---------- 71

LIST OF FIGURES

1. Kaman ROTOCHUTE ---------- 16

2. Study Vehicle Configuration ---------- 23

3. Blade Section Forces ---------- 24

4. Rotor Geometry ---------- 24

5. Typical Low-speed Operating Characteristics -------- 34

6. Operating Characteristics from Newtonian Theory ---- 34

7. Comparison of Theoretical and Experimental Rotor Drag Coefficient ---------- 35

8. Drag Coefficient vs. Mach (Nonlifting; $D_r/D_o = 2$) -- 37

9. Drag Coefficient vs. Mach (Lifting; $D_r/D_o = 2$) ----- 38

10. L/D vs. Mach (Lifting; $D_r/D_o = 2$) ---------- 39

11. Typical Range Footprints ($\gamma = -3^{\circ}$; $D_r/D_o = 2$) ----- 41

12. Maximum Deceleration ($D_r/D_o = 2$) ---------- 43

13. Rotor Blade Maximum Heating Rate vs. Re-entry Angle - 44

14. Effect of Diameter Ratio on Lateral Range ---------- 47

15. Effect of Diameter Ratio on Longitudinal Range ----- 49

16. Effect of Diameter Ratio on Deceleration ---------- 50

17. Rotor Blade Maximum Heating Rate (Nonlifting; $R_o = 1.524$ m) ---------- 51

18. Rotor Blade Maximum Heating Rate (Lifting; $R_o = 1.524$ m) ---------- 52

19. Diameter Ratio vs. Maximum Blade Temperature (Nonlifting; $R_o = 1.524$ m) ---------- 54

20. Diameter Ratio vs. Maximum Blade Temperature (Lifting; $R_o = 1.524$ m) ---------- 55

21. Lateral Range vs. Deployment Mach Number ($\gamma = -3^{\circ}$; $D_r/D_o = 2$) ---------- 57

22. Lateral Range vs. Deployment Mach Number
(γ = -3°; D_r/D_o = 4) ---------- 58

23. Longitudinal Range vs. Deployment Mach Number
(γ = -3°; D_r/D_o = 2) ---------- 59

24. Stagnation-point Wall Temperature vs. Mach Number
(γ = -2°; D_r/D_o = 4) ---------- 61

25. Rotor Vehicle Operating Modes ---------- 62

26. Rotor Entry Vehicle System ---------- 67

GLOSSARY

BTU	British Thermal Unit(s)
^{o}F	degree(s) Fahrenheit
ft	foot (feet)
fps	feet per second
g	an acceleration unit equal to 32.17 fps^{2}
IBM	International Business Machines
in.	inch(es)
^{o}K	degree(s) Kelvin
kg	kilogram(s)
KW	kilowatt(s)
lb	pound(s)
m	meter(s)
NASA	National Aeronautics and Space Administration
nmi	nautical mile(s)
rpm	revolutions per minute
'Struth	God's Truth

NOTATION

A_c capsule area, $\pi D_c^2/4$

A_r rotor disk area, πR^2

b number of blades

C_c' maximum value of c_x

C_D drag coefficient, $\dfrac{\text{drag}}{(1/2)\rho V_\infty^2 A_c}$

C_{Dr} rotor drag coefficient, $\dfrac{\text{rotor drag}}{(1/2)\rho V_\infty^2 A_r}$

C_L lift coefficient, $\dfrac{\text{lift}}{(1/2)\rho V_\infty^2 A_c}$

C_{m_X} rolling-moment coefficient, $\dfrac{M_x}{(1/2)\rho V_\infty^2 A_r R}$

C_{m_Y} pitching-moment coefficient, $\dfrac{M_y}{(1/2)\rho V_\infty^2 A_r R}$

C_N' maximum value of variable portion of c_n

C_{No} value of c_n at $\alpha_s = 0^\circ$

C_Q rotor torque coefficient, $\dfrac{Q}{(1/2)\rho V_\infty^2 A_r R}$

C_X axial-force coefficient, $\dfrac{X}{(1/2)\rho V_\infty^2 A_r}$

C_Y side-force coefficient, $\frac{Y}{(1/2)\rho V_\infty^2 A_r}$

C_Z normal-force coefficient, $\frac{Z}{(1/2)\rho V_\infty^2 A_r}$

c blade chord

c_n blade section normal force coefficient

c_x blade section chord force coefficient

D diameter

dm blade mass element

e flapping hinge offset

F_P blade local force normal to surface swept by the rotor

F_T blade local force tangent to surface swept by the rotor

h_e re-entry altitude

I_1 blade moment of inertia about flapping hinge

L/D lift-drag ratio

M_A aerodynamic moment about flapping hinge

M_{CF} centrifugal moment about flapping hinge

M_X rolling moment

M_Y pitching moment

M_∞ free-stream Mach number

m	blade mass per unit length
m_o	blade mass at the root
m_r	blade mass at the tip
Q	rotor torque
$\dot{q}$	heating rate
R	rotor radius
R_e	local blade radius of curvature
r	blade spanwise station, measured from flapping hinge
T	radiation equilibrium temperature
U	local velocity
U_P	local velocity component at blade normal to surface swept by rotor
U_T	local velocity component at blade tangent to surface swept by rotor
$\dot{V}$	deceleration
V_e	re-entry velocity
V_∞	free-stream velocity
W	vehicle weight
X	axial force

Y	side force
Z	normal force
α	rotor angle of attack
α_s	blade section local angle of attack
β	flapping angle
γ	re-entry angle relative to the local horizontal, positive up
δ	m_r/m_o
ε	emissitivity
η,λ	constants used in expression for blade-section chord-force coefficient
θ	blade collective pitch angle
ν	Stefan-Boltzmann constant
ξ	e/R
ρ	mass density of air
σ	rotor solidity
ϕ	bank angle
χ	r/R

ψ	azimuth angle of blade, measured from most aft position
Ω	rotor rotational speed

Subscripts

c	capsule
r	rotor
r+c	rotor plus capsule
max	maximum

I. INTRODUCTION

A. GENERAL

Initially, the United States manned spaceflight efforts used ballistic re-entry of blunt-body vehicles followed by parachute landings at sea for recovery. This technique was the most expedient at the time, but the enormous requirement for recovery assets and their coordination along with the high cost of the single-use designs proved to be prohibitive. The space shuttle concept (following the abortive X-20 *DynaSoar* project), that of using a modified blunt body with a modest Lift/Drag (L/D) ratio, allows re-entry to culminate in landings at specific ground locations and solves many of the problems associated with nominal blunt-body re-entry. However, the high landing speeds required limit the number of suitable landing areas. Emergency landings on water, uneven terrain, or during inclement weather have little chance of success. Therefore, as a step toward the solution of these problems, a blunt-body re-entry vehicle incorporating a deployable rotor system for recovery was studied.

Space vehicles equipped with a rotor for entering the atmosphere from orbit offer several advantages over other re-entry techniques, some of which are unique to rotary wings alone. The rotor recovery system has the potential of

being the only system which in one unit can perform the functions of drag modulation, stabilization, flight path control through improved maneuverability, and landing with near zero vertical and horizontal speeds on an unprepared landing site, thereby making the recovery of spacecraft more precise, safe, and economical.

Numerous investigators have reported on the rotor recovery technique. Kretz [Ref. 1] discussed the application of rotors to atmospheric entry and recovery problems. Hodson [Ref. 2] discussed the results of low-speed wind tunnel tests on a 12- and 14-ft-diameter rotor system. Barzda and Schultz [Ref. 3] reported on the results of a series of free-flight drop tests and wind tunnel tests at supersonic speeds of a rotary-wing decelerator. Other aspects of the rotary-wing recovery technique can be found in References 4 through 6, inclusive.

From the literature on the subject of rotary-wing decelerators, it was found that nearly all of the studies considered using the rotor only for the final approach and touchdown maneuver. Only a few considered deploying the rotor at transonic speeds, even though wind tunnel tests had been conducted to a Mach number of about 3 [Ref. 3]. Only Kretz [Ref. 1] had considered deploying a lifting rotor at the time of re-entry into the atmosphere. Since the rotor has to be carried into orbit for use later during the touchdown maneuver, it became clear that the rotor might

also prove useful throughout the entire re-entry trajectory for modulating drag, reducing deceleration through added lift, and providing increased lateral range capability. An analytical investigation was undertaken to estimate the rotor aerodynamic characteristics, and then these were used in combination with a re-entry vehicle to determine what gains in performance might be achieved over those of a lifting capsule alone for re-entry from earth orbit.

B. SPECIFIC

The rotor derives the advantages described above from the fact that the energy it stores during autorotation constitutes the means of providing lift. Many of these advantages have been demonstrated with the Kaman ROTOCHUTE, shown in Figure 1 [Ref. 7].

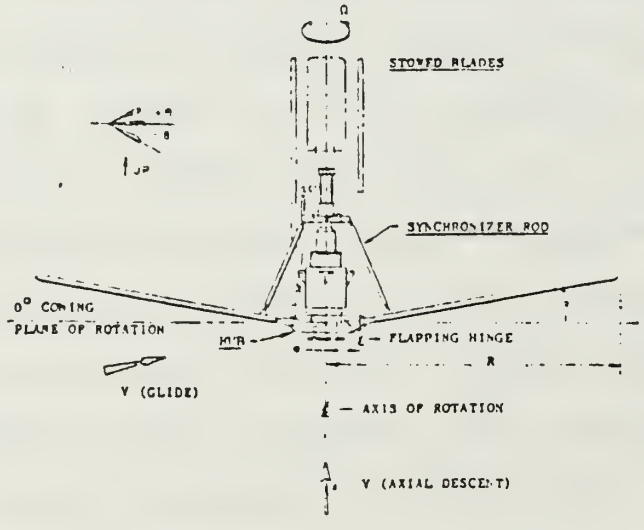

Figure 1

Kaman ROTOCHUTE [Ref. 7]

The ROTOCHUTE design, combined with the blunt-body concept, prompted this investigation. It incorporates a governor mechanism that limits the rotor speed to its design norm throughout deployment, retardation, and descent. Other major elements are:

* folding, stowable blades that provide the retarding force, are pitch controlled, and can flap through 90°
* the rotor hub, which houses the rotational bearings and provides blade attachment with flapping and pitch freedom
* linkages that synchronize the coning of the blades during deployment to minimize rotational imbalance
* a static line or explosive cartridge actuated deployment initiator that unlocks the hub and positions the blades for aerodynamic spin-up of the rotor system
* the support shaft connecting the rotor assembly and the vehicle.

Folded in the trail position during spaceflight, the rotor would be deployed at the onset of entry into the atmosphere. When the dynamic pressure became large enough, the rotor would be set into rotation with a large coning angle which would be gradually decreased to near-zero at low-subsonic speeds. (Coning of all blades during opening is kept equal by the synchronizing system.) As the centrifugal force increased, the rotor blades would open farther into the airstream, increasing the rotational rate which, in turn, would cause the blades to open still farther. Finally, equilibrium would be reached when the

centrifugal moment equals the aerodynamic moment. Thus, the rotor needs only the oncoming airstream to effect full deployment of the blades.

C. PRINCIPLES OF OPERATION

1. Axial Descent

When the system's drag essentially equals the vehicle weight, the system will be at its terminal or equilibrium rate of descent. The drag coefficient varies with flight speed, rotor solidity, and blade coning, and is maximum at low speed or advance ratio. At low flight speed, most of the blade operates efficiently as an unstalled airfoil, and the resulting lift is high.

As the inflow speed increases, the inflow angle increases, and the blade stalls over more of its span, the stall progressing outward toward the tip. The force coefficient then becomes smaller with increasing speed until it reaches a relatively constant value when the blades become fully stalled and act essentially as "drag plates".

At the higher speeds, when the retardation force is a function of the "drag plate" area, the drag coefficient is nearly proportional to rotor solidity. At low speeds, solidity influences the speed more at which the maximum drag coefficient is attained rather than the actual value. Speed for the maximum drag coefficient is less at lower solidity; however, a lower limit is placed on rotor solidity by blade

stall considerations. A compromise is therefore required in the choice of blade solidity for specific applications.

The "drag plate" area of the rotor is also influenced by blade coning. The exposed area becomes smaller with increased coning. Thus, modulation of the retardation force is possible by controlling rotor speed, which in turn influences the blade coning angle. With modulation, the re-entry deceleration may be regulated within limits, rates of descent may be varied, and down-range landing points may be controlled.

2. Glide Flight

With control, a rotary wing decelerator can be put into glide autorotative descent in the same manner as a helicopter with the power off. The angle of the glide path relative to the horizon is primarily dependent on the glide speed or advance ratio, blade pitch angle, and system parasite drag. The addition of a payload vehicle increases the system parasite drag, steepening the glide path angle. The influence is more pronounced at higher speeds.

An important consideration during glide is an inherent tendency for most rotor systems to roll when in forward flight. The rolling moment can, however, be satisfactorily trimmed through lateral control.

3. Touchdown

The total energy of a rotor system in descent is composed of its potential energy due to altitude, kinetic

energy due to the velocity of the mass, and the rotational energy in the rotor. This energy can be used to substantially retard the horizontal and vertical velocities for touchdown. The kinetic energy of translation is used for "cyclic" flare, whereas the rotational energy of the rotor is used for "collective" flare.

Cyclic flare is performed by commanding an aft tilt of the rotor. This maneuver not only tilts the rotor force vector aft, but increases the force by tending to speed up the rotor. The speed-up may be permitted, if so desired, or the blade pitch can be increased to maintain rotor speed constant. Either action will increase the rotor lift or retardation. The tilted and increased force resolves into components retarding the horizontal and vertical velocities.

Collective flare also may be used alone or in conjunction with cyclic flare to retard the vertical descent. By commanding a rapid and collective increase of blade pitch to near-stall values, a transient increase in rotor lift is produced. This action causes rotor rpm to drop off. Thus, flare performance is dependent on rotor kinetic energy, i.e., on rotor rpm at the beginning of the maneuver and the inertia of the rotor. The greater either one is, the longer will be the transient increase.

If the collective flare is performed after glide and cyclic flare, the vertical rate of descent will have been retarded partially, leaving less work to be performed by the

rotor in collective flare. Collective flare from vertical descent may be desirable in certain applications; however, for the purpose herein examined (in which weight is a primary consideration), the advantage of a smaller and lighter rotor provided by the combination flare technique is significant.

II. THEORY

A. INTRODUCTION

The aerodynamic characteristics of the rotor alone were analyzed for use in combination with the aerodynamic characteristics of a nominal capsule shape [Ref. 8]. The analysis was very similar to the approach taken in References 9 through 12 which was based upon blade element theory with Newtonian flow concepts used to represent the local blade forces. Small angle approximations were made on the blade collective pitch angle, θ . In the analysis presented herein, however, no small-angle assumptions were made in regard to the collective pitch angle so that angles up to 90° might be considered. The equations thus obtained were solved numerically on an IBM 3033 mainframe computer system.

Figure 2 presents the rotor-plus-capsule configuration selected for this study, while Figures 3 and 4 show the blade forces and rotor geometry, respectively. The geometrical relations shown in Figures 3 and 4 were used to obtain the aerodynamic characteristics of the rotor alone. The equations obtained are presented herein, without the steps required to go from the integral form to the analytic solution, to provide a basis for future investigation while at the same time avoiding tedium. For the force

representation assumed, the integration is relatively straightforward. In general, if the blade section forces cannot be expressed in the form assumed herein, solving the integral equations would require stepwise numerical integration.

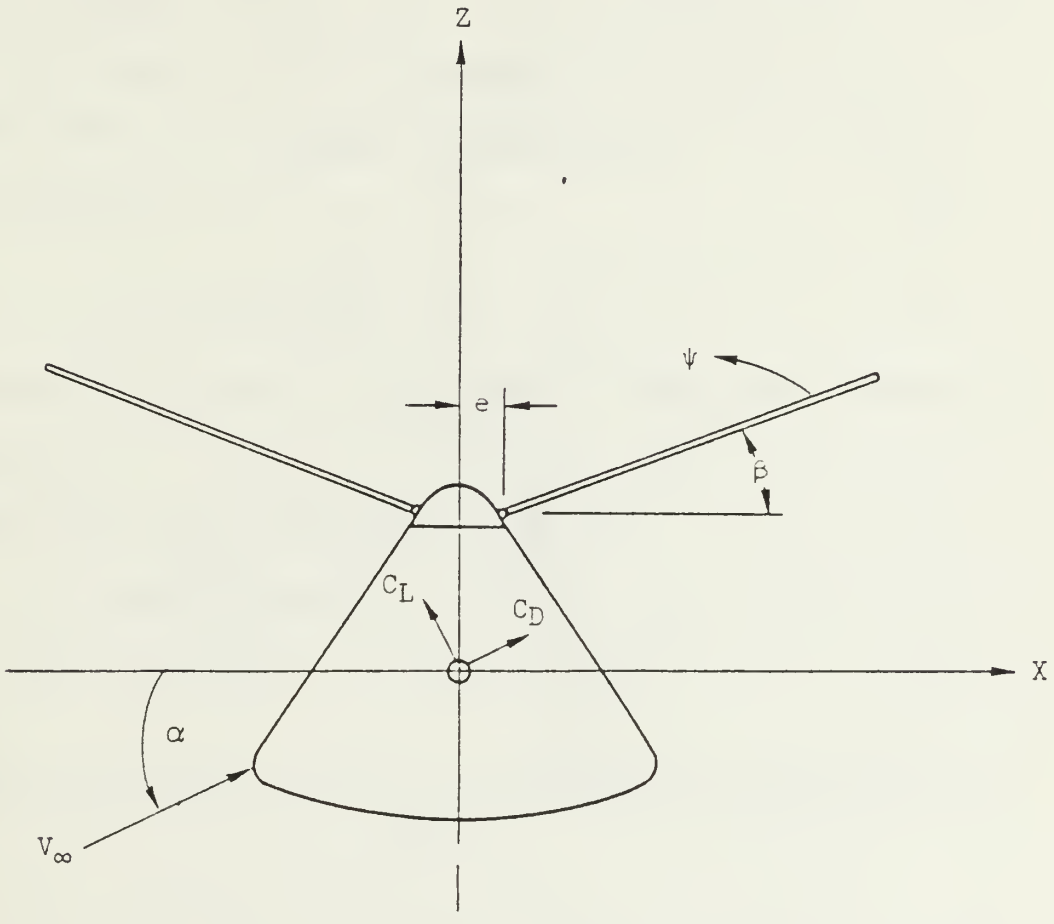

Figure 2

Study Vehicle Configuration

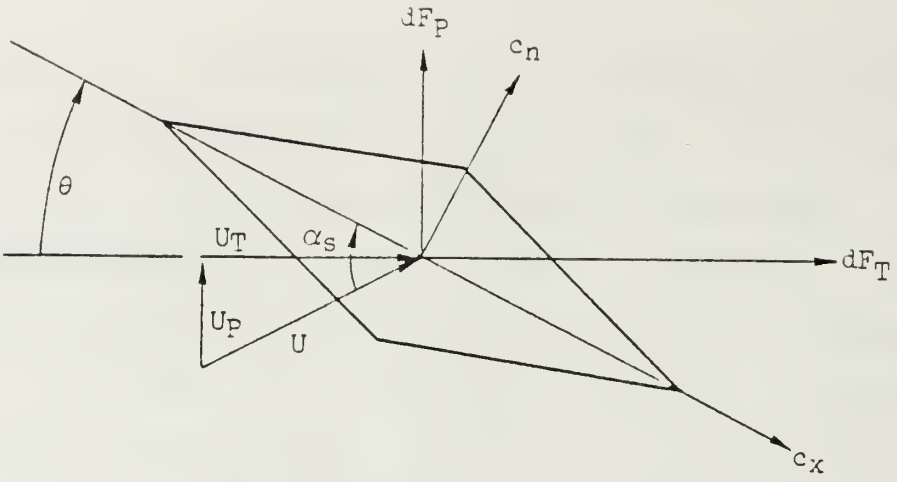

Figure 3

Blade Section Forces

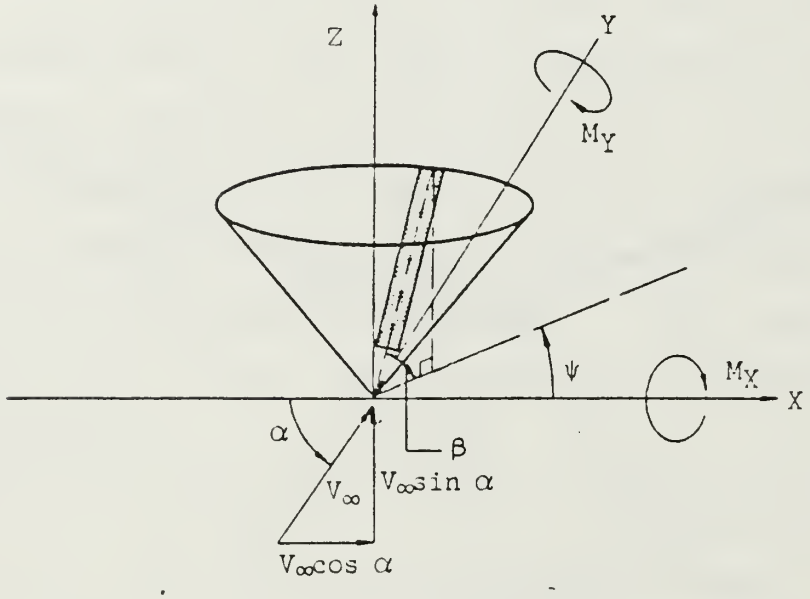

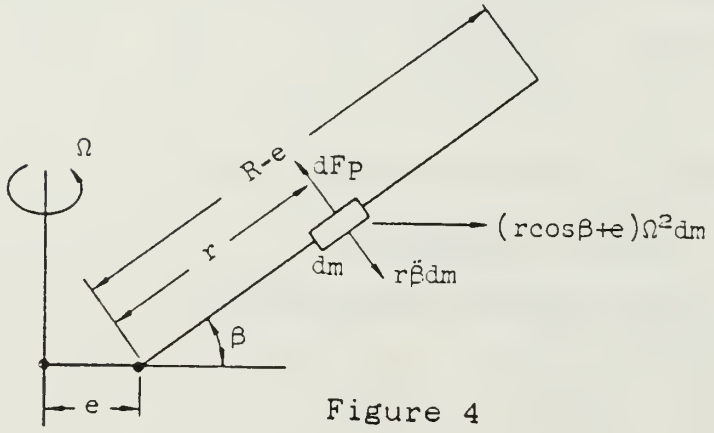

Figure 4

Rotor Geometry

For the rotor system considered, the local velocities and section angle of attack are obtained from Figures 3 and 4:

$$U_P = V_\infty (\sin\alpha \cos\beta - \cos\alpha \sin\beta \cos\psi) \quad (1)$$

$$U_T = \Omega R \{\chi \cos\beta + \xi + (V_\infty/\Omega R) \cos\alpha \sin\psi\} \quad (2)$$

$$\alpha_s = \theta + \tan^{-1}(U_P/U_T) \quad (3)$$

where it has been assumed that $r\ddot{\beta} = 0$ (synchronizer linkage forces all blades to have the same coning angle, β).

The blade section normal and chord forces are assumed to be of the form:

$$c_n = C_{No} + C_N' \sin^2\alpha_s \quad (4)$$

$$c_x = C_c' (\cos^2\alpha_s - \lambda \sin^2\alpha_s - \eta) \quad (5)$$

This form of the forces may be used to represent Newtonian flow forces.

The local blade forces are given by:

$$dF_P = (1/2)\rho c R U^2 (c_n \cos\theta - c_x \sin\theta)\, d\chi \quad (6)$$

$$dF_T = (1/2)\rho c R U^2 (c_n \sin\theta + c_x \cos\theta)\, d\chi \quad (7)$$

The following useful forms are obtained from Equation (3):

$$U^2 \sin^2\alpha_s = U_P^2 \cos^2\theta + 2U_P U_T \sin\theta \cos\theta + U_T^2 \sin^2\theta \quad (8)$$

$$U^2 \cos^2\alpha_s = U_T^2 \cos^2\theta - 2U_P U_T \sin\theta \cos\theta + U_P^2 \sin^2\theta \quad (9)$$

where

$$U^2 = U_P^2 + U_T^2 \quad (10)$$

B. DERIVATION OF OPERATING CHARACTERISTICS

Rotor torque is obtained by integrating the elemental aerodynamic torque about the rotor axis:

$$Q = (bR/2\pi) \int_0^{2\pi} \int_0^{1-\xi} (dF_T/d\chi)(\chi \cos\beta + \xi)\, d\chi\, d\psi \qquad (11)$$

Substituting Equations (1), (2), (4), (5), and (10) into Equation (11), performing the indicated integration assuming β is constant and dividing by $(1/2)\rho V_\infty^2 \pi R^3$ results in the expression for the rotor torque coefficient.

$$C_Q = \sigma(1-\xi)\Big[\{C_N' \sin^3\theta + C_c' \cos\theta(\cos^2\theta - \lambda\sin^2\theta - \eta) + C_{No}\sin\theta\}$$

$$\{[(1-\xi)^3/4]\cos^3\beta + \xi(1-\xi)^2\cos^2\beta + (3/2)\xi^2(1-\xi)\cos\beta + \xi^3\}(\Omega R/V_\infty)^2$$

$$+ \{C_{No}\sin\theta + C_c'\cos\theta(\sin^2\theta - \lambda\cos^2\theta - \eta) + C_N'\sin\theta\cos^2\theta\}$$

$$\{\sin^2\alpha\cos^2\beta + (\cos^2\alpha\sin^2\beta)/2\}\{[(1-\xi)/2]\cos\beta + \xi^2\}$$

$$+ \sin 2\theta \sin\alpha\cos\beta(\Omega R/V_\infty)\{C_N'\sin\theta - C_c'\cos\theta(1+\lambda)\}$$

$$\{[(1-\xi)^2/3]\cos^2\beta + \xi(1-\xi)\cos\beta + \xi^2\} + \{(\cos^2\alpha)/2\}$$

$$\{C_{No}\sin\theta + C_c'\cos\theta(\cos^2\theta - \lambda\sin^2\theta - \eta) + C_N'\sin^3\theta\}$$

$$\{[(1-\xi)/2]\cos\beta + \xi\}\Big| \qquad (12)$$

The blade centrifugal moment is given by:

$$M_{CF} = R^2 \int_0^{1-\xi} (\chi\cos\beta + \xi)\,\chi\sin\beta\,\Omega^2\, dm \qquad (13)$$

For a blade with a linear mass distribution:

$$m = m_o\{1 - (1-\delta)\chi/(1-\xi)\} \qquad (14)$$

where

$$\delta = m_r/m_o \qquad (15)$$

and

$$dm = mR\, d\chi \qquad (16)$$

Substituting Equations (14), (15), and (16) into Equation (13) gives:

$$M_{CF} = I_1 \Omega^2 \sin\beta \{[(1 + 3\delta)/4] \cos\beta + [(1 + 2\delta)\xi)/2(1 - \xi)\} \quad (17)$$

where

$$I_1 = [(m_o R^3 (1 - \xi)^3]/3 \quad (18)$$

The aerodynamic moment that tends to raise the coning of one blade is given by:

$$M_A = (R/2\pi) \int^{2\pi} \int^{1-\xi} (\chi dF_P/d\chi)\, d\chi\, d\psi \quad (19)$$

The integrated expression for the aerodynamic moment is:

$$M_A = (1/4)\rho c R^4 \Omega^2 (1 - \xi)^2 \cos\theta \Big[\{(C_{No} + C_N' \sin^2\theta) + C_c' \tan\theta (\eta + \lambda \sin^2\theta - \cos^2\theta)\} \{[(1 - \xi)^2/2] \cos^2\beta + (4/3)\xi (1 - \xi) \cos\beta + \xi^2 + (V_\infty/\Omega R)^2 (\cos^2\alpha)/2\} + \{(C_{No} + C_N' \cos^2\theta) + C_c' \tan\theta (\eta + \lambda \cos^2\theta - \sin^2\theta)\} (V_\infty/\Omega R)^2 \{\sin^2\alpha \cos^2\beta + (\cos^2\alpha \sin^2\beta)/2\} + \sin 2\theta \sin\alpha \cos\beta (V_\infty/\Omega R) \{C_N' + C_c' (1 + \lambda) \tan\theta\} \{(2/3)(1 - \xi) \cos\beta + \xi\}\Big] \quad (20)$$

For equilibrium coning $M_{CF} = M_A$ and for autorotative torque equilibrium $C_Q = 0$; thus, there are two equations in the three unknowns, β, θ, and $\Omega R/V_\infty$. The collective pitch angle (θ) is chosen as the independent variable, and the equations for β and $\Omega R/V_\infty$ are solved. The results are substituted into the expressions which follow to determine the aerodynamic force coefficients.

C. DERIVATION OF AERODYNAMIC PERFORMANCE CHARACTERISTICS

The rotor axial, side, and normal forces, respectively, are

$$X = (b/2\pi) \int_0^{2\pi} \int_0^{1-\xi} \{ (dF_T/d\chi) \sin \psi - (dF_P/d\chi) \sin \beta \cos \psi \} \, d\chi \, d\psi \qquad (21)$$

$$Y = (-b/2\pi) \int_0^{2\pi} \int_0^{1-\xi} \{(dF_P/d\chi) \sin \beta \sin \psi + (dF_T/d\chi) \cos \psi \} \, d\chi \, d\psi \qquad (22)$$

$$Z = (b/2\pi) \int_0^{2\pi} \int_0^{1-\xi} \{(dF_P/d\chi) \cos \beta \, d\chi \, d\psi \qquad (23)$$

Integrating and dividing by $(1/2) \rho V_\infty^2 \pi R^2$ gives the rotor axial, side, and normal force coefficients:

$$C_X = \sigma \cos \alpha (1-\xi) \Big[\{ \sin \theta (C_{N_0} + C_{N'} \sin^2 \theta) + C_{c'} \cos \theta (\cos^2 \theta - \lambda \sin^2 \theta \cos^2 \beta - \eta) \} (\Omega R/V_\infty) \{ [(1-\xi)/2] \cos \beta + \xi \} + \{ (C_{N'} \tan \theta - C_{c'}) \sin \theta \cos^2 \theta + (C_{N'} \cos^3 \theta - C_{c'} \sin^3 \theta) \sin^2 \beta - C_{c'} \lambda \sin \theta \cos^2 \theta \cos^2 \beta \} \sin \alpha \cos \beta + (C_{N_0} \cos \theta + C_{c'} \eta \sin \theta) \sin \alpha \sin^2 \beta \cos \beta + (C_{N'} + C_{c'} \tan \theta) (\Omega R/V_\infty) \sin \theta \cos^2 \theta \sin^2 \beta \Big] \qquad (24)$$

$$C_Y = \sigma \cos \alpha \sin \beta \cos \theta (1-\xi) \Big[\{ C_{c'} \{ (\sin 2\theta)/2 \} (1 - \lambda \sec^2 \theta) - C_{N'} \sin^2 \theta - C_{c'} \eta \tan \theta - C_{N_0} \} (\Omega R/V_\infty) \{ [(1-\xi)/2] \cos \beta + \xi \} + \{ C_{N_0} \tan \theta - C_{c'} (\eta + \lambda) \} \sin \alpha \cos \beta + (C_{N'} \sin \theta - C_{c'} \cos \theta) (\Omega R/V_\infty) \sin \theta \Big] \qquad (25)$$

$$C_Z = \sigma \cos^3 \beta \cos \theta (1-\xi) \Big[\{ C_{N_0} + C_{N'} \sin^2 \theta + C_{c'} (\eta \tan \theta - \sin \theta \cos \theta + \lambda \sin^2 \theta \tan \theta \} (\Omega R/V_\infty)^2 \{ [(1-\xi)^2/3] + \xi (1-\xi) \sec \beta + \xi^2 \sec^2 \beta \} + \{ C_{N_0} + C_{N'} \cos^2 \theta + C_{c'} \tan \theta (\eta - \sin^2 \theta + \lambda \cos^2 \theta) \} \{ \sin^2 \alpha + \cos^2 \alpha (\tan^2 \beta)/2 \} + \{ C_{N_0} + C_{N'} \sin^2 \theta + C_{c'} \tan \theta (\eta - \cos^2 \theta + \lambda \sin^2 \theta) \} \{ (\cos^2 \alpha)/2 \} \sec^2 \beta + 2 \sin \theta \sin \alpha (\Omega R/V_\infty) \{ C_{N'} \cos \theta + C_{c'} (1+\lambda) \sin \theta \} \{ [(1-\xi)/2] + \xi \sec \beta \} \Big] \qquad (26)$$

The rotor rolling and pitching moment about the hub are

$$M_X = (-bR/2\pi) \int_0^{2\pi} \int_0^{1-\xi} \{(dF_P/d\chi)(\chi + \xi \cos\beta) \sin\psi + (dF_T/d\chi) \sin\beta \cos\psi\} \, d\chi \, d\psi \quad (27)$$

$$M_Y = (bR/2\pi) \int_0^{2\pi} \int_0^{1-\xi} \{(dF_T/d\chi) \sin\beta \sin\psi - (dF_P/d\chi)(\chi + \cos\beta) \cos\psi\} \, d\chi \, d\psi \quad (28)$$

Integrating and dividing by $(1/2)\rho V_\infty^2 \pi R^3$ gives the rotor rolling and pitching moment coefficients about the hub:

$$C_{m_X} = -\sigma \cos\alpha \cos\theta \cos\beta (1-\xi)^2 \left[\{C_{N'} + C_c'(1+\lambda)\tan\theta\}\{(\sin 2\theta)/2\} \sin\alpha \{(1/2) + \{\xi/(1-\xi)\}\cos\beta\}\right.$$
$$+ \{C_{No} + C_{N'} \sin^2\theta + C_c' \tan\theta (\eta - \cos^2\theta + \lambda \sin^2\theta)\}(\Omega R/V_\infty)$$
$$\{\{(1-\xi)/3\} + \{\xi/2\} \sec\beta (1 + \cos^2\beta) + \xi^2/(1-\xi)\}$$
$$- \{C_{No} \tan\theta - C_c'(\eta + \lambda \cos^2\theta) + (C_{N'} + C_c' \tan\theta)\{(\sin 2\theta)/2\}\{(\sin\alpha)/2\} \sin^2\beta$$
$$\left. - \{C_{N'} \tan\theta - C_c'(1+\eta)\}\{(\sin 2\theta)/2\} \sin^2\beta (\Omega R/V_\infty)\{\{(1-\xi)/3\} + \{\xi/2\} \sec\beta\}\right] \quad (29)$$

$$C_{m_Y} = \sigma \cos\alpha \cos\theta \{(\sin 2\beta)/2\}(1-\xi^2)\left[\{C_{N'} + C_c' \tan\theta (1+\lambda)\}\{(\sin 2\theta)/2\}(\Omega R/V_\infty)\right.$$
$$\{(1-\xi)/3 + \{\xi/2\} \sec\beta (1 + \cos^2\beta) + \xi^2/(1-\xi)\}$$
$$+ \{\tan\theta (C_{No} + C_{N'} \sin^2\theta) + C_c' (\cos^2\theta - \lambda \sin^2\theta - \eta)\}(\Omega R/V_\infty)\{(1-\xi)/3 + \{\xi/2\} \sec\beta\}$$
$$+ \{C_{No} + C_{N'} \cos^2\theta + C_c' \tan\theta (\eta - \sin^2\theta + \lambda \cos^2\theta)\}\{(1/2) + \xi \cos\beta/(1-\xi)\} \sin\alpha$$
$$\left. + \{(\sin 2\theta)/4\} \sin\alpha \{C_{N'} \tan\theta - C_c'(1+\lambda)\}\right] \quad (30)$$

The rotor lift/drag ratio is computed from:

$$L/D = (C_Z \cos\alpha - C_X \sin\alpha)/(C_X \cos\alpha + C_Z \sin\alpha) \quad (31)$$

D. THEORETICAL SOLUTION FOR AXIAL FLOW

For the special case of $\alpha = 90^{\circ}$ (the nonlifting case), $\delta = 1$ and $C_{No} = \eta = \lambda = \xi = 0$, the equations reduce to a very simplified form. Here no simultaneous solution of equations is required to obtain the equilibrium values for β and $\Omega R/V_{\infty}$, and the equations become:

$$C_Q = \sigma \cos^3 \beta \{[C_N' \tan^3 \theta + C_c'][\Omega r/V_{\infty}]^2 + [8/3][C_N' \tan^2 \theta - C_c' \tan \theta] + 2[C_N' \tan \theta + C_c' \tan^2 \theta]\} \quad [32]$$

$$M_{CF} = [I_1 \Omega^2/2] \sin 2\beta \quad [33]$$

$$M_A = [1/4] \rho c R^4 \Omega^2 \{[1/2] \tan \theta [C_N' \tan \theta - C_c'] + [C_N' - C_c' \tan^3 \theta][V_{\infty}/\Omega R]^2 + [4/3] \tan \theta [C_N' + C_c' \tan \theta][V_{\infty}/\Omega R]\} \quad [34]$$

$$C_Z = \sigma \cos^3 \beta \cos^3 \theta \{[[\tan \theta]/3][C_N' \tan \theta - C_c'][\Omega R/V_{\infty}]^2 + [C_N' - C_c' \tan^3 \theta] + \tan \theta [C_N' + C_c' \tan \theta][\Omega R/V_{\infty}]\} \equiv C_D \quad [35]$$

Equation (32) is solved for the equilibrium value of $\Omega R/V_{\infty}$ as a function of θ, independent of the value of β. Equation (33) is equated to Equation (34) and the value of $\Omega R/V_{\infty}$ obtained from Equation (32) is used to find the equilibrium coning angle, β.

E. VEHICLE PERFORMANCE CHARACTERISTICS

1. Aerodynamic Characteristics

The results from the theoretical analysis of aerodynamic characteristics of the rotor alone were combined with the capsule aerodynamic characteristics in order to obtain the combined rotor-plus-capsule characteristics. The capsule area is used as the reference area since it remains constant, whereas the rotor disk area may vary as a result of coning. For the lifting re-entry the results were combined linearly, as follows:

$$C_{D_{r+c}} = C_{D_c} + C_{D_r}\frac{A_r}{A_c}$$

$$\left(\frac{L}{D}\right)_{r+c} = \frac{C_{L_c} + C_{L_r}(A_r/A_c)}{C_{D_{r+c}}}$$

For the nonlifting re-entry, since the vehicle is aligned with the flight path, a first-order interference correction to account for the area shielded by the capsule was made to the combined drag coefficient of the rotor-plus-capsule as follows:

$$C_{D_{r+c}} = C_{D_c} + C_{D_r}\left(\frac{A_r}{A_c} - 1\right)$$

2. Atmospheric Re-entry Performance

An adaption of an available computer code [Ref. 9] was used to obtain the re-entry trajectory parameters. This three-dimensional program included the effects of the earth's oblateness and rotation, and it was assumed that the

earth's atmosphere rotated with the earth. The aerodynamic characteristics obtained from the above relations were programmed as tabulated functions of the relative velocity (i.e., of the velocity relative to the rotating atmosphere).

III. RESULTS AND DISCUSSION

A. INTRODUCTION

To analyze the performance characteristics of a rotor re-entry vehicle it was first necessary to obtain the rotor operating characteristics. Once these characteristics had been determined, the present theory was used to obtain the rotor aerodynamic characteristics for the conditions of autorotative equilibrium. Then these aerodynamic characteristics were used to determine the vehicle re-entry performance characteristics.

B. ROTOR OPERATING CHARACTERISTICS

Figures 5 and 6 show typical variations of equilibrium dimensionless tip speed with blade pitch. Figure 5 shows a low-speed operating characteristic which is typical of known data. Note that for the blade pitch range -6° to $+9^{\circ}$ the tip speed is multi-valued, hence an unstable operating range exists. Figure 6 shows tip speed data for supersonic flight. Data for the values of the ratio C_N/C_c are shown for axial flight ($\alpha = 90^{\circ}$) as well as one value for $\alpha = 20^{\circ}$. The ratio C_N/C_c is a measure of the ratio of the elemental driving force to the retarding force. This ratio for an airfoil in Newtonian flow equals the chord-to-thickness ratio. Axial flight produced the highest

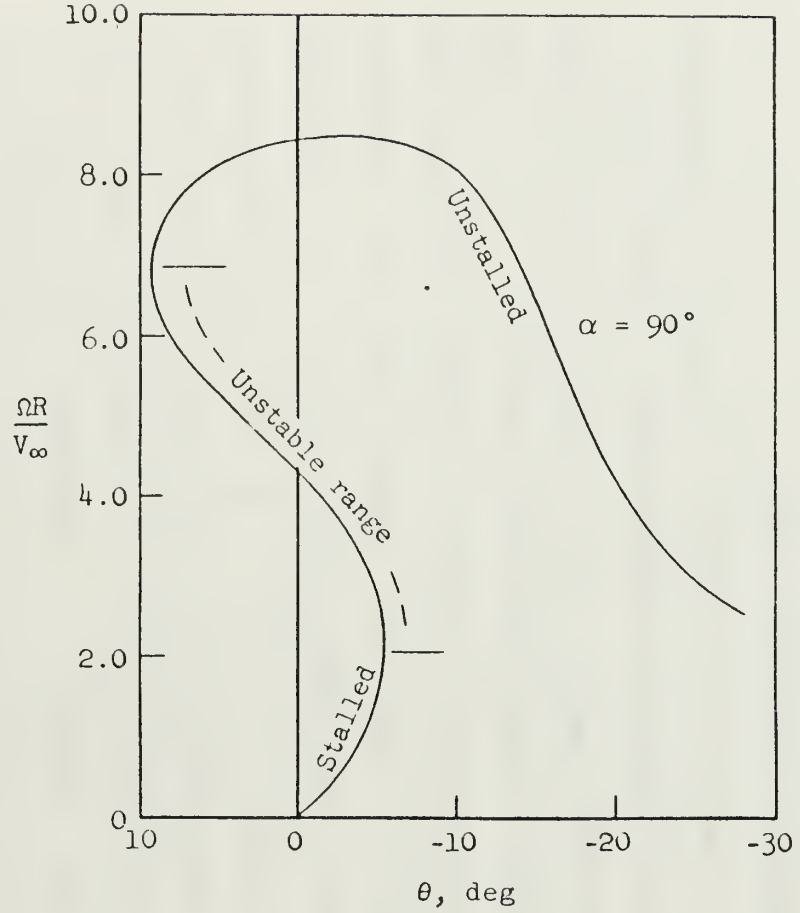

Figure 5

Typical Low-speed
Operating Characteristics

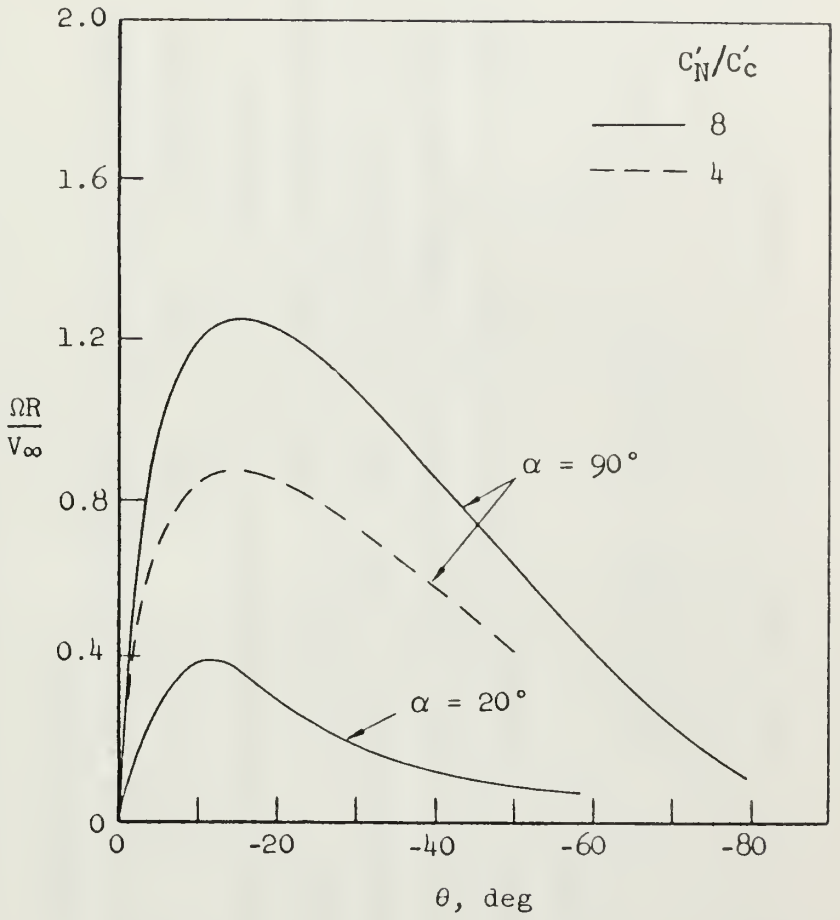

Figure 6

Operating Characteristics
from Newtonian Theory

[Source: Ref. 1]

rotor speeds and the greatest sensitivity to pitch change near zero pitch. Accordingly, very accurate pitch control will be needed in this range during axial flight in order to avoid accidental overspeeding. These predicted rotor speeds are single-valued and hence stable for any blade pitch angle, something that was not apparent from low-speed rotor characteristics.

C. ROTOR AERODYNAMIC CHARACTERISTICS

Figure 7 shows a comparison of theoretical and experimental rotor drag coefficients for the configuration of Reference 3 as a function of Mach number for a rotor in axial flight at a tip speed of 107 m/sec (350 fps).

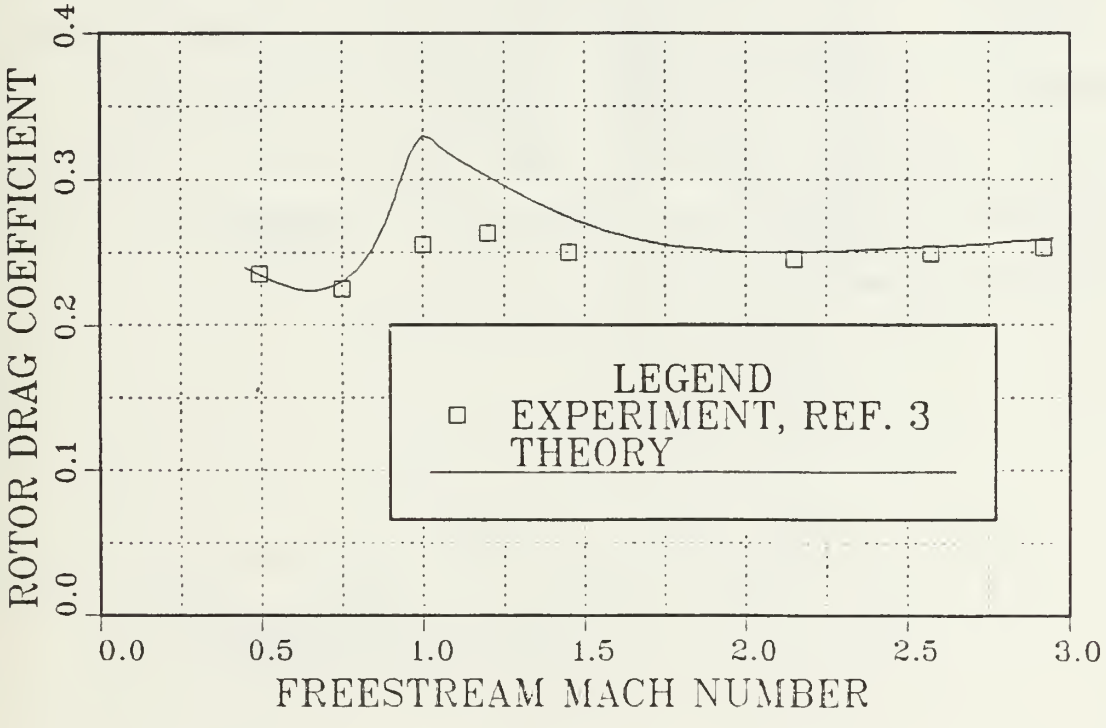

Figure 7

Comparison of Theoretical and Experimental Rotor Drag Coefficient

D. VEHICLE RE-ENTRY PERFORMANCE CHARACTERISTICS

1. Introduction

Figures 8, 9, and 10 show comparisons between the capsule and rotor-plus-capsule aerodynamic performance characteristics obtained from data contained in References 9--12. These characteristics were used in the trajectory program to obtain re-entry performance parameters, such as maximum deceleration, range, and heating rates; Figures 11, 12, and 13 present the significant results. The capsule-alone configuration was also investigated to provide a basis for comparison. The hypothetical full-scale capsule has a maximum diameter of 3.96 m (13 ft) and weighs 4,535 kg (9,400 lb). The rotor system selected has four blades, a solidity of 0.2, and a diameter of 7.82 m (26 ft). The initial re-entry conditions used were V_{∞} = 7,610 m/sec (25,000 fps) and h_{∞} = 121,920 m (400,000 ft); initial re-entry angles were varied from 0° to -3°.

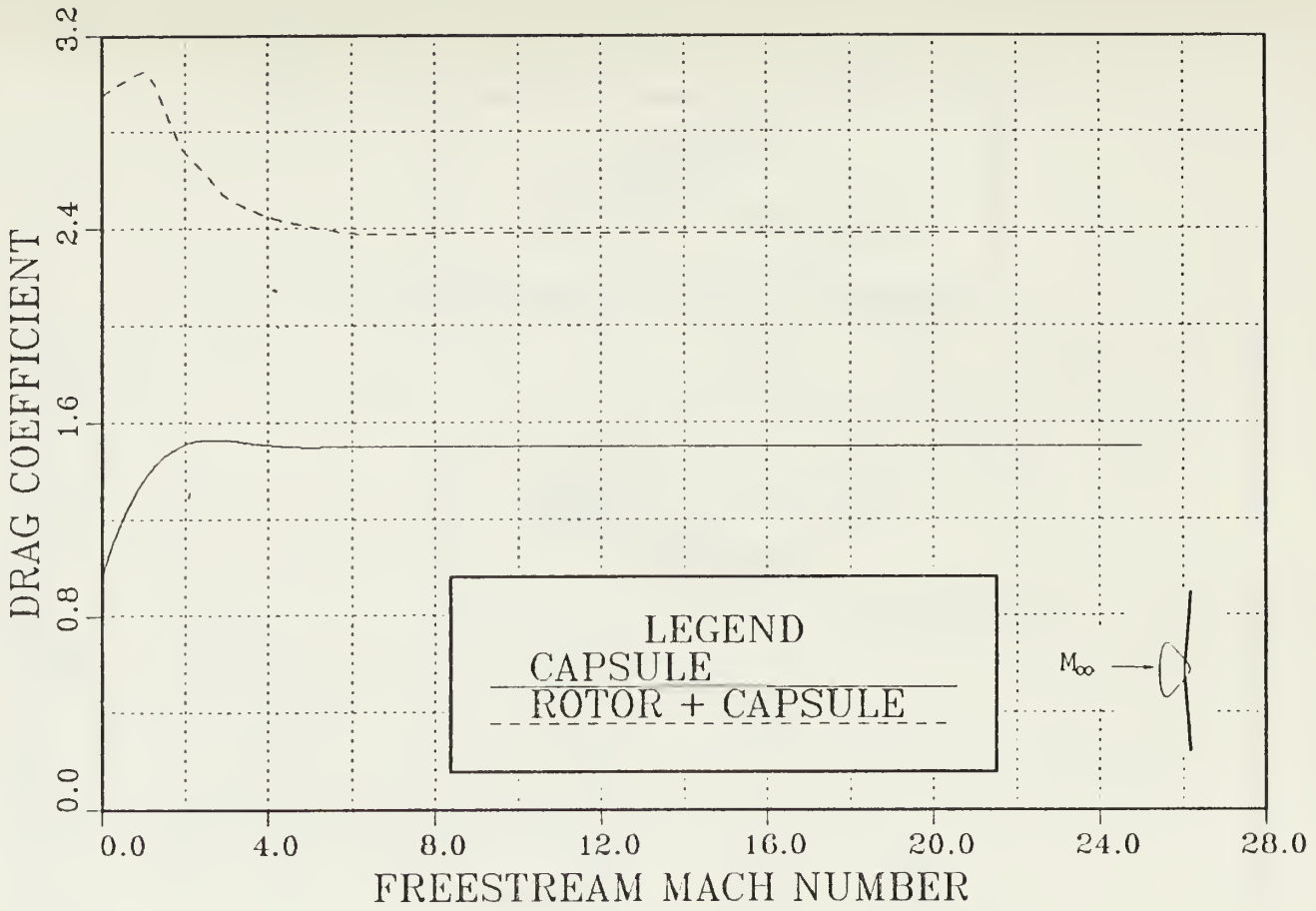

Figure 8

Drag Coefficient vs. Mach (Nonlifting; $D_r/D_c = 2$)

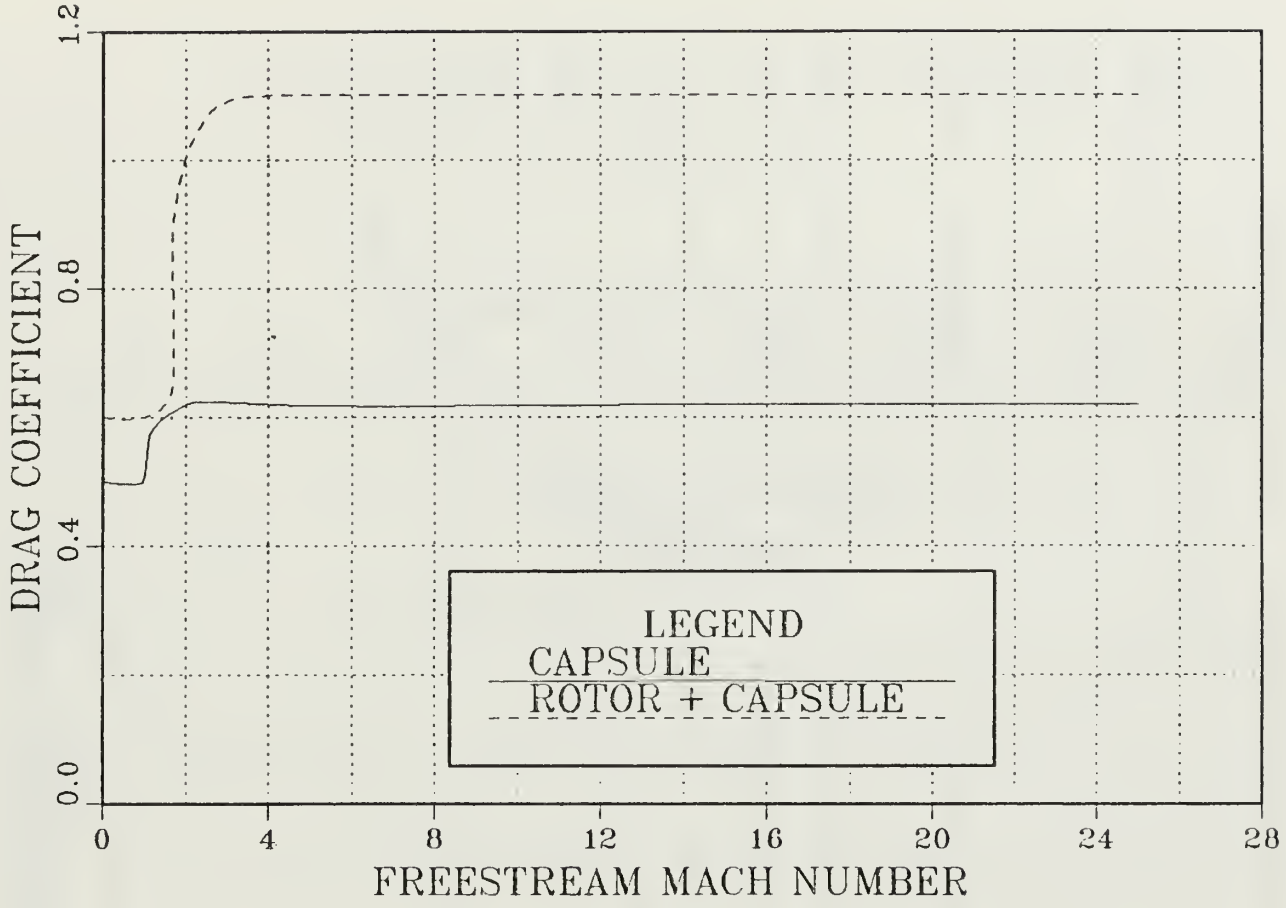

Figure 9

Drag Coefficient vs. Mach (Lifting; D_r/D_C = 2)

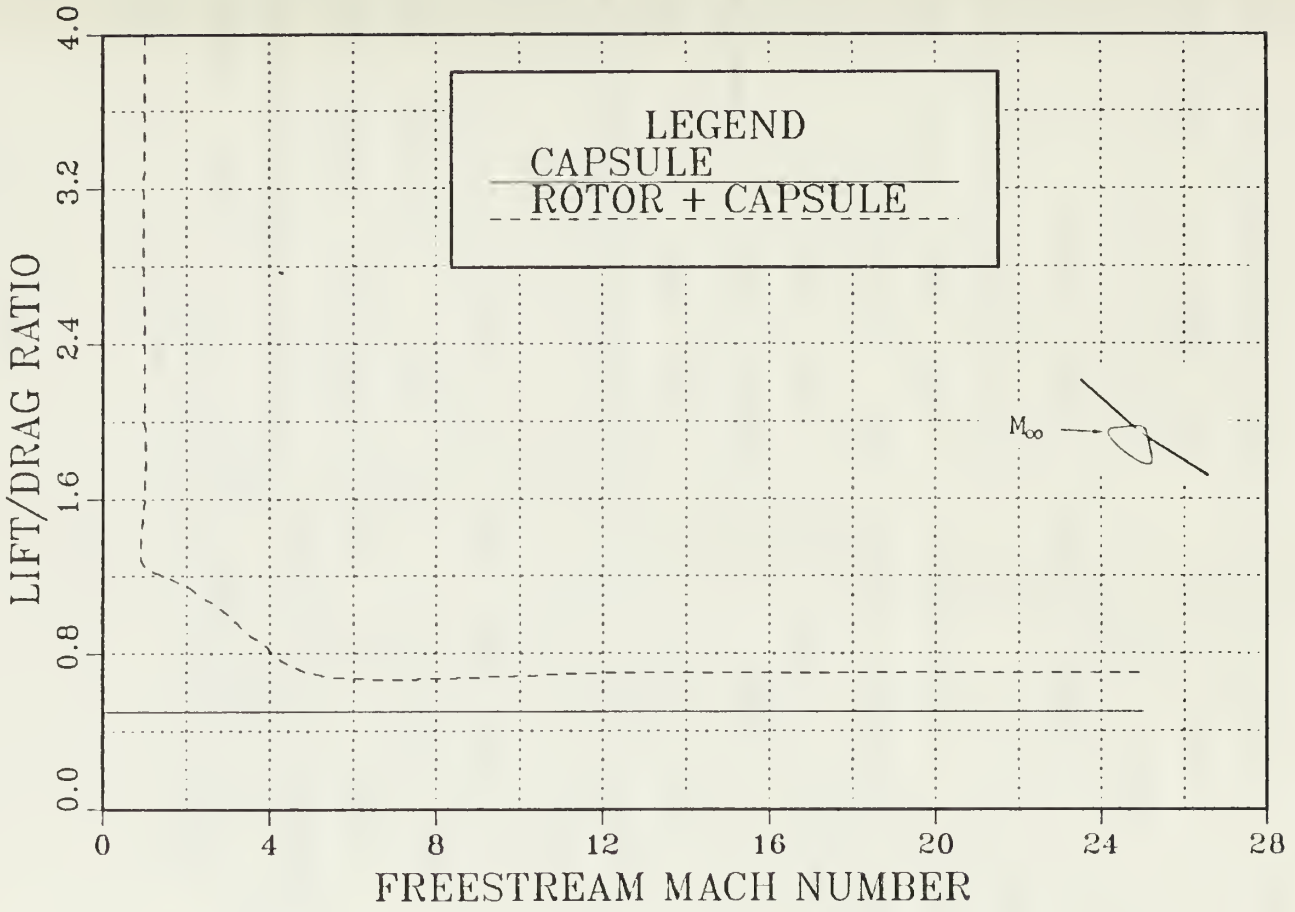

Figure 10

L/D vs. Mach (Lifting; $D_r/D_c = 2$)

2. Range

Figure 11 shows the range footprints for the lifting capsule and lifting rotor-plus-capsule for a re-entry angle of -3°. Also indicated on the figure for comparison is the maximum lateral range for L/D = 1.2, which is obtainable with lifting bodies such as the NASA Ames M-2. The reference for all ranges indicated is the impact point for the nonlifting capsule. The available landing area for the rotor-plus-capsule configuration is about eight times larger than for the lifting capsule alone. The maximum lateral range is extended from about 210 to nearly 520 nmi by the addition of the rotor. The maximum lateral range was obtained by rolling the vehicle to a bank angle of 45° and maintaining this attitude until the heading changed 90° from the re-entry heading. At that time the vehicle was rolled back to a 0° bank angle and the glide continued until touchdown. The addition of the rotor increased the longitudinal range of the capsule from about 1200 to over 1900 nmi. However, this increase is not so significant as the lateral range increase, since to a large extent longitudinal range can be controlled by adjusting the time of retrofire.

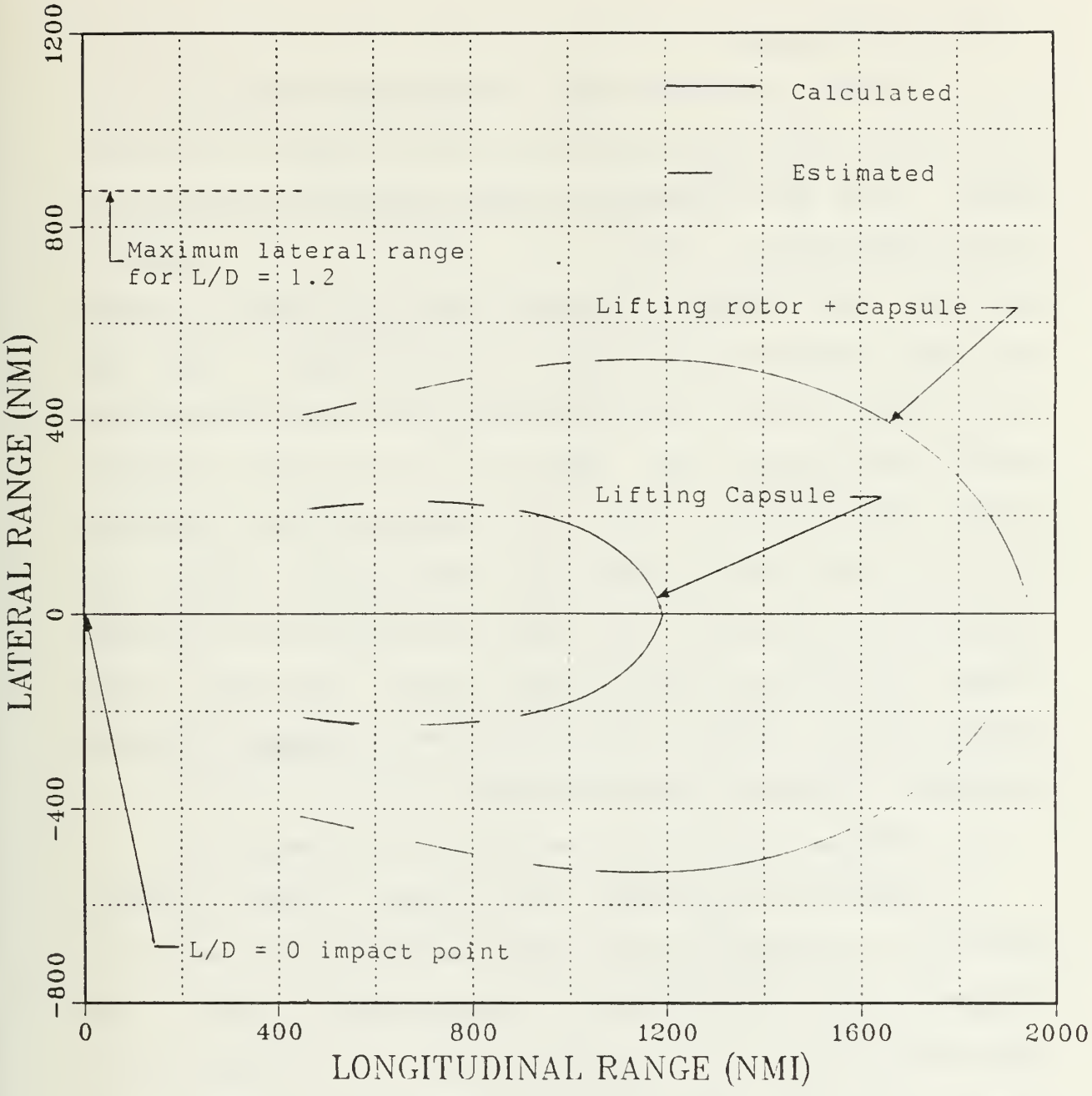

Figure 11

Typical Range Footprints ($\gamma = -3^0$; $D_r/D_c = 2$)

3. Deceleration

Figure 12 shows the maximum deceleration for the lifting and nonlifting re-entries as a function of re-entry angle. They are presented only to show the trends which result from adding a rotor to a capsule. As would be expected, the maximum decelerations encountered increased with the steepening of the re-entry angle. For the nonlifting re-entry, the addition of the rotor reduced the maximum deceleration only about Ø.5 g for all re-entry angles investigated. For the lifting re-entry, adding a rotor to the capsule did not significantly change the maximum deceleration. Note that the addition of the rotor changes the ballistic coefficient, $W/C_DA_\square$, from that for the capsule alone. Hence, the curves shown on Figure 12 do not represent a constant value of $W/C_DA_\square$.

4. Heating (Calculation method from Reference 13)

Figure 13 presents the rotor blade maximum convective heating rate as a function of re-entry angle for lifting and nonlifting trajectories of the rotor-plus-capsule and capsule alone. No magnification effects due to the capsule bow shock are included. The heating rates presented are for a local blade radius of curvature of Ø.152 m (6 in.) for the lifting re-entry and 1.524 m (5 ft) for the nonlifting re-entry. Radiative heating rates were not computed, but they have been shown to contribute a negligible amount to the overall heating for

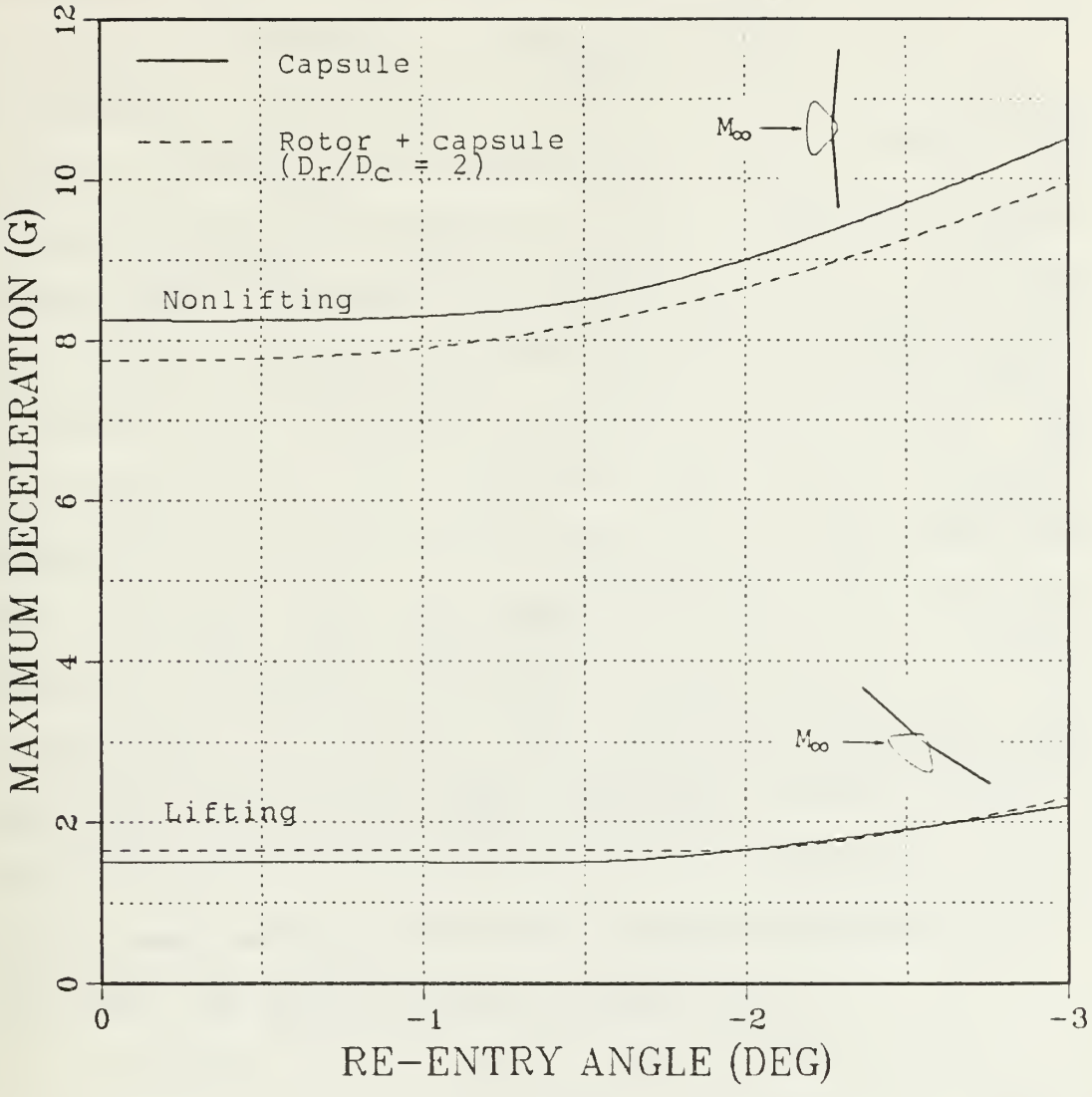

Figure 12

Maximum Deceleration (D_r/D_c = 2)

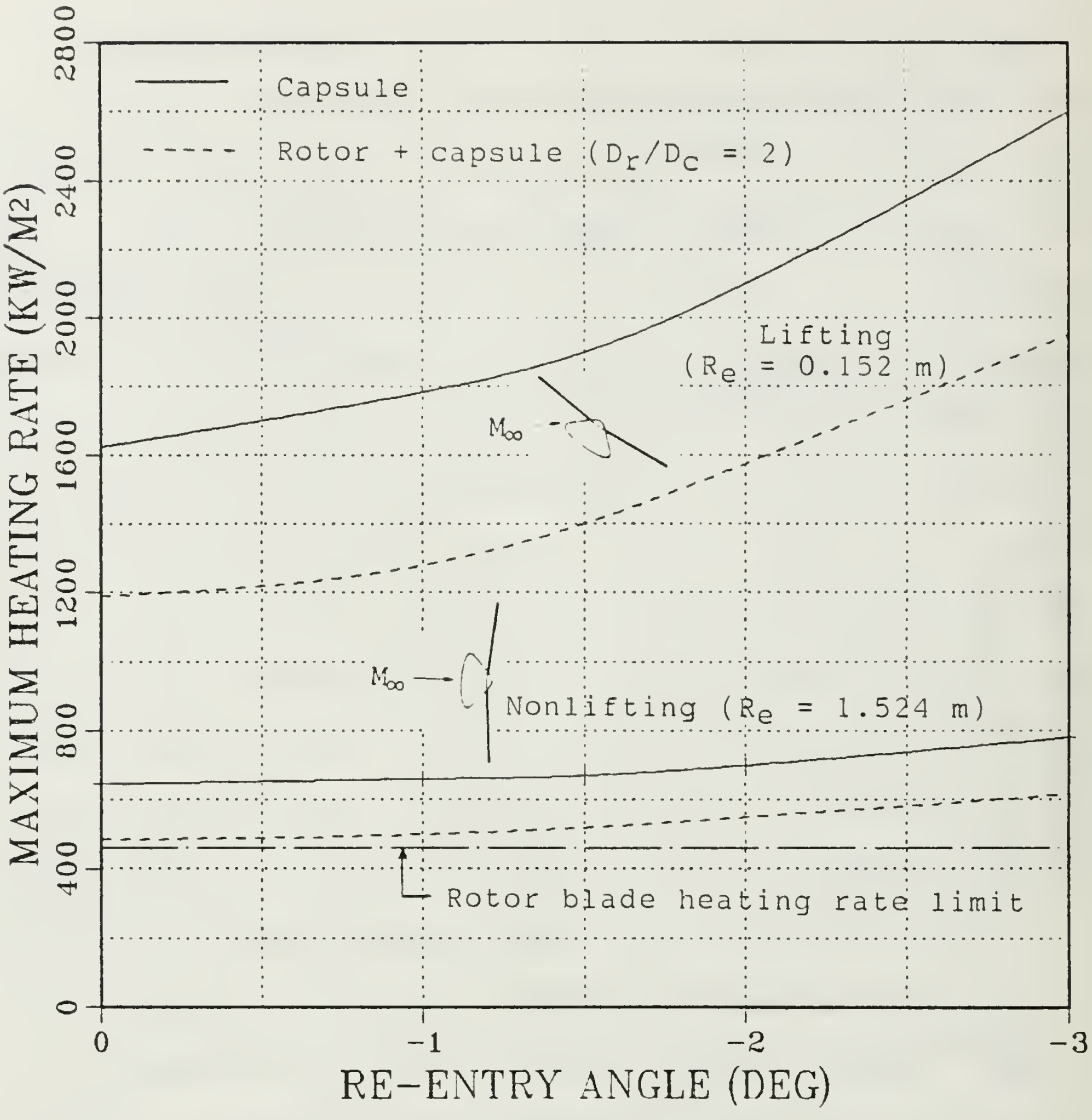

Figure 13

Rotor Blade Maximum Heating Rate vs. Re-entry Angle

re-entry at low earth orbital speeds [Ref. 13]. A line on the figure indicates the maximum heating rate limit, 463 kW/m^2 (41 BTU/ft^2/sec). This limit is based on a radiation equilibrium temperature of 2320 ^{o}K (3700 ^{o}F) and has been adjusted by a factor of 2.85 to account for the increase in blade heating behind the capsule bow shock wave. This temperature limit is for a RENE-41 blade structure with a stabilized zirconium oxide coating (chosen for its availability and historical use). This coating is assumed to be satisfactory for operation in this temperature range. It has also been assumed that the coating is sufficient to maintain the RENE-41 structure below its limit of about 1087 ^{o}K (1500 ^{o}F). It can be seen from the figure that even for re-entry at 0^{o}, the blade heating rate is too severe. It is also evident from the nonlifting re-entry curves that adding the rotor reduces the maximum heating rate about 20% for all re-entry angles studied.

Because of the severe nature of the heating of the rotor blades, an investigation was undertaken to determine if increasing the rotor-to-capsule diameter ratio would appreciably reduce the heating rates. An increase in D_r/D_c reduces W/C_DA_c and should reduce the heating rates. The significant results of the effect of diameter ratio on the re-entry parameters is discussed in the next section. Of course, the utilization of state-of-the-art alternative materials for the blade structure might improve the rotor

resistance to heating; time available for this study did not allow consideration of alternate materials.

5. Effects of Diameter Ratio on Range, Deceleration, and Heating

Figure 14 shows the maximum lateral range as a function of diameter ratio for various re-entry angles. A diameter ratio of 1 represents the capsule alone. There is a very significant effect of diameter ratio up to about $D_r/D_c = 4$. Above this value, the gain is not nearly so significant and from a weight standpoint further increases in rotor diameter probably would not be worth the small gain in lateral range. This gain can be attributed to increased lift due to the increase in rotor size. For the range of re-entry angles investigated, the maximum lateral range was insensitive to re-entry angle, the maximum difference being only about 22 nmi.

It should be noted that autorotative landing studies show that the maximum disk loading tolerable for a reasonable subsonic sink rate (hence, a reasonably safe landing) also requires a D_r/D_c in the neighborhood of 3 or more. Increasing $D_r/D_c = 2$ to 4 results in about 180 nmi of additional range, an increase of about 47%. Whether the increase in range is worth the increased weight and more difficult stowage problem of the larger rotor will depend upon mission requirements. However, rotors providing $D_r/D_c = 6$ or more would probably not be suitable.

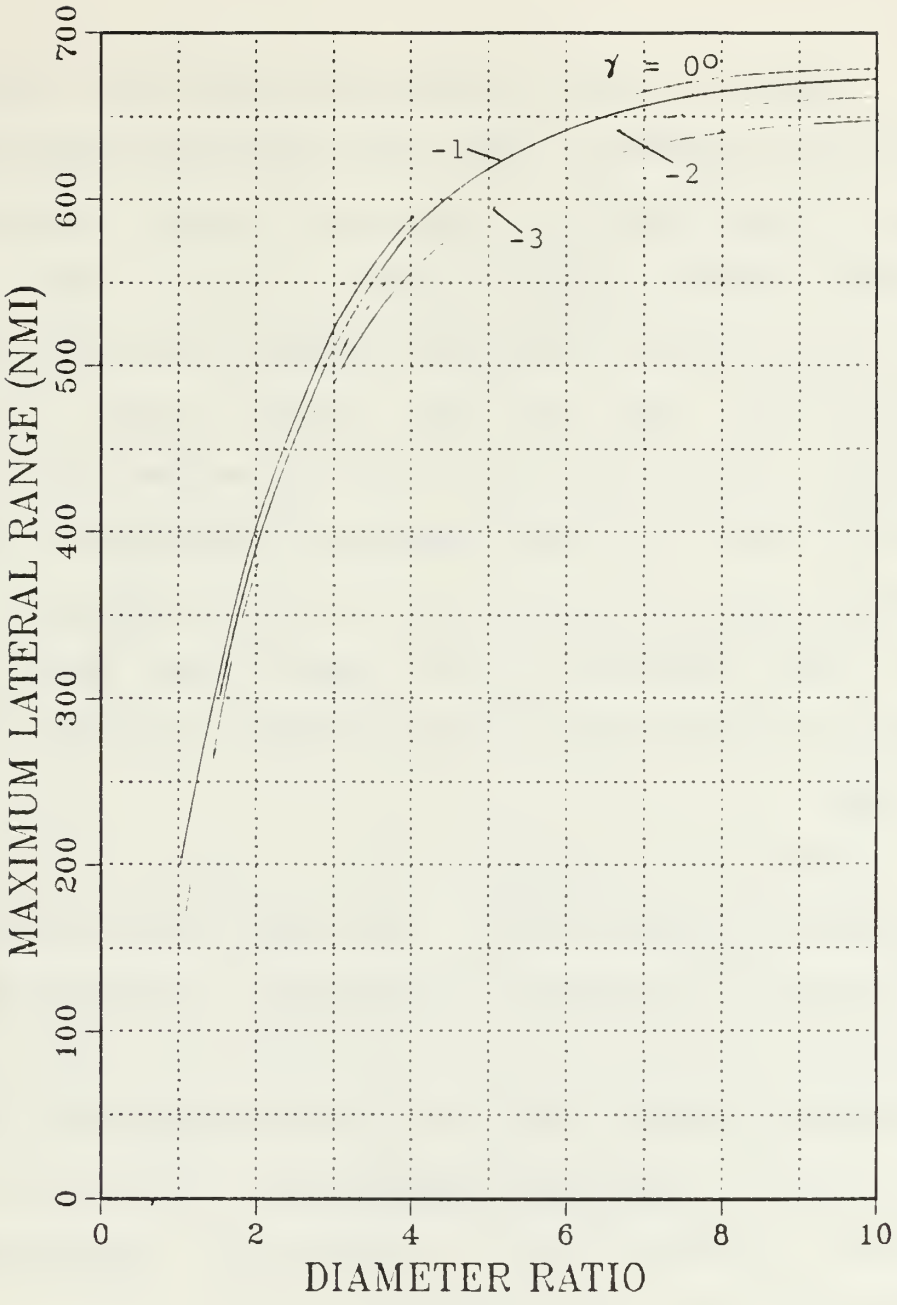

Figure 14

Effect of Diameter Ratio on Lateral Range

Figure 15 shows the maximum longitudinal range as a function of diameter ratio for the four re-entry angles studied. These ranges were measured from the capsule-alone ballistic impact point, which varied with re-entry angle. The maximum longitudinal range is more sensitive to re-entry angle than was the lateral range, as would be expected. From the figure it can be seen that the effect of diameter ratio on the maximum longitudinal range is generally the same as it is for the maximum lateral range. For diameter ratios larger than about 4, the increase in range with further increase in diameter ratio is very small.

Figure 16 presents the maximum deceleration encountered during re-entry. For nonlifting re-entry there is a minimum in the maximum deceleration encountered at a diameter ratio of about 3.5; this minimum is a result of the effect of the W/C_DA_c. For the lifting re-entry the maximum deceleration is greatly reduced from the values for the nonlifting re-entry and is essentially unaffected by diameter ratio for a given re-entry angle.

Figures 17 and 18, respectively, show the rotor blade maximum convective heating rates for the nonlifting and lifting re-entries studied. It can be seen that the effect of increasing the diameter ratio is to reduce markedly the heating rate for both the nonlifting and lifting re-entries. A vehicle with a diameter ratio of

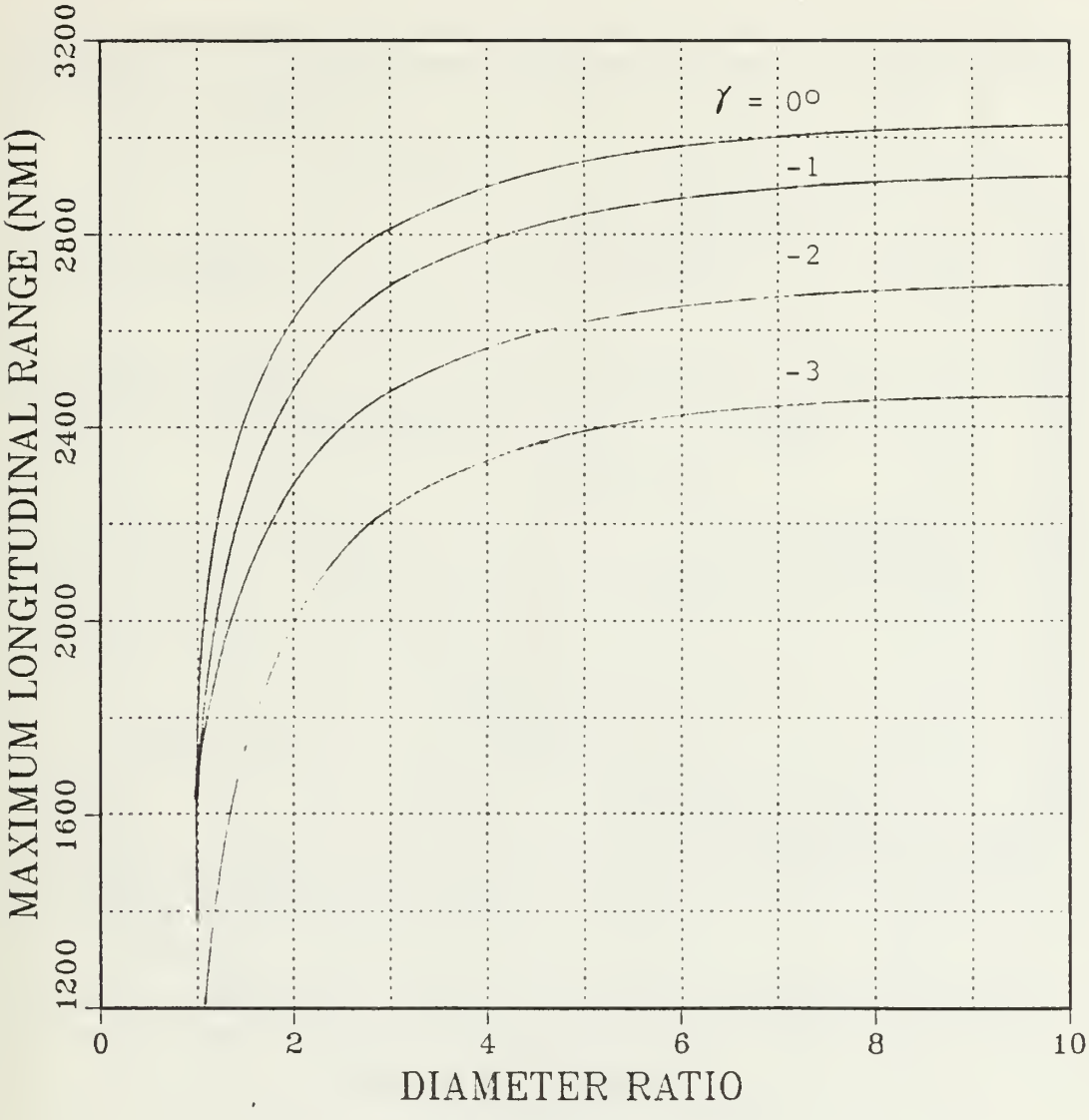

Figure 15

Effect of Diameter Ratio on Longitudinal Range

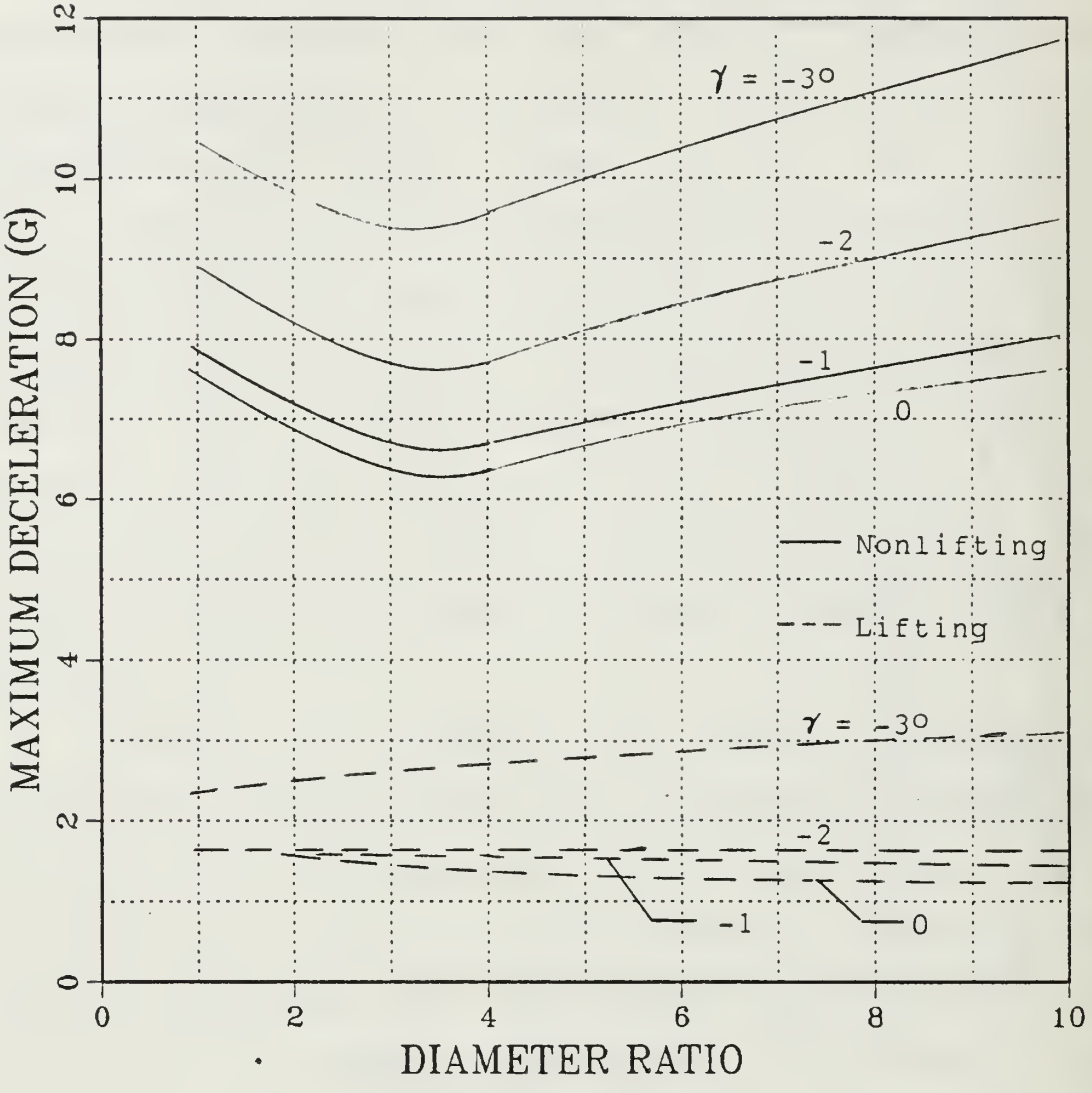

Figure 16

Effect of Diameter Ratio on Deceleration

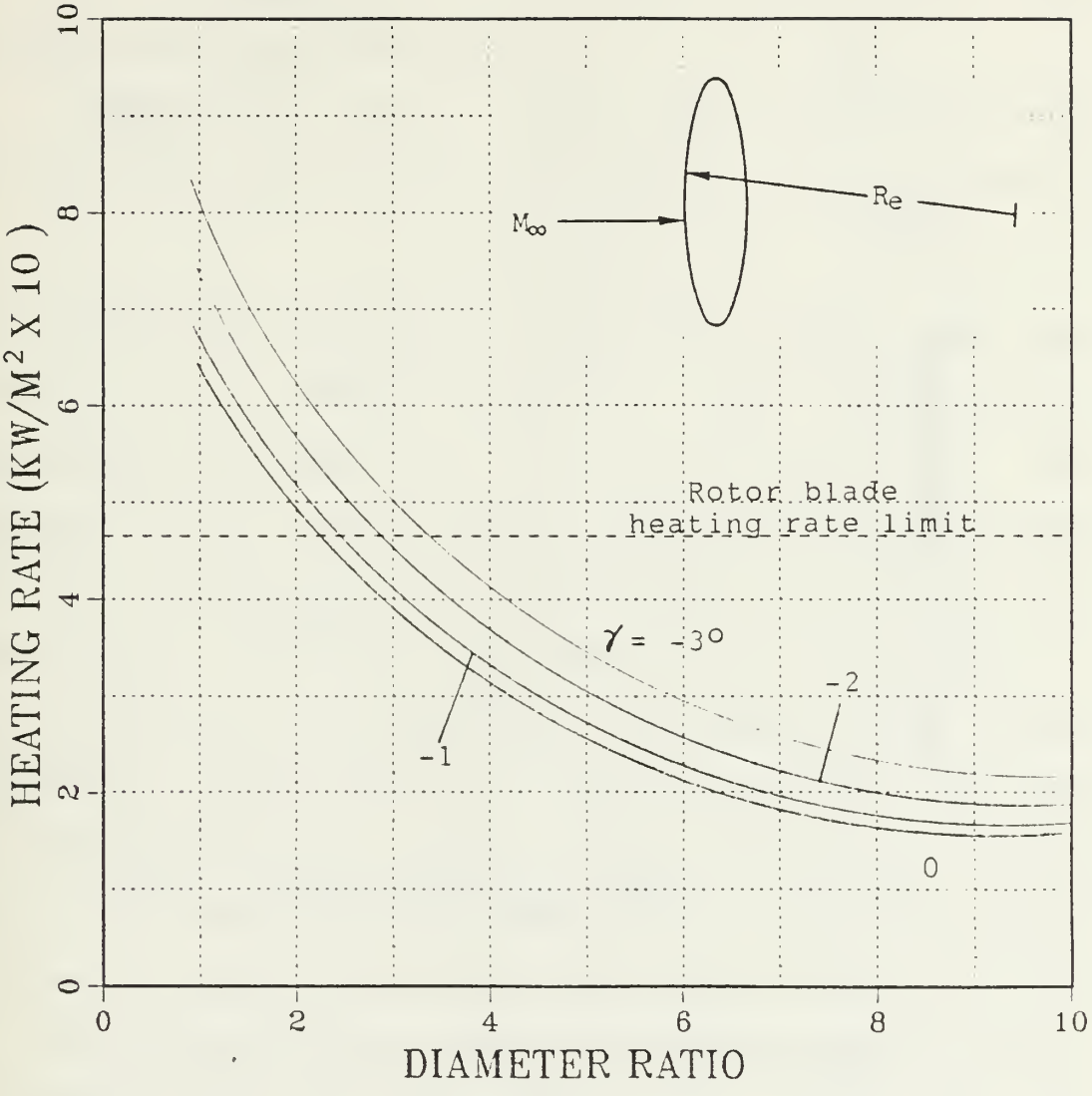

Figure 17

Rotor Blade Maximum Heating Rate
(Nonlifting; R_e = 1.524 m)

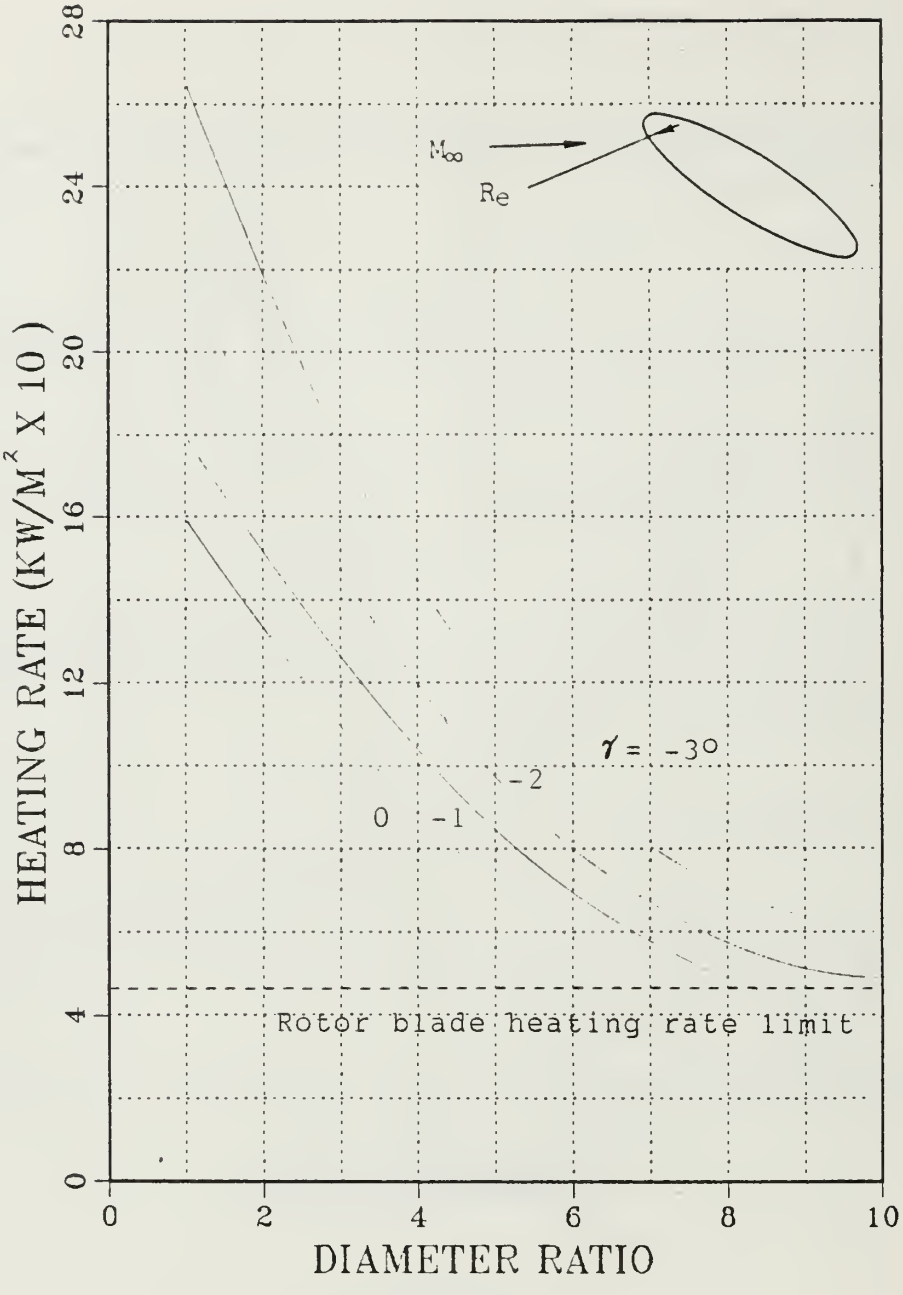

Figure 18

Rotor Blade Maximum Heating Rate
(Lifting; R_e = 1.524 m)

about 4 has approximately half the maximum blade heating rate it would have if it were re-entering on the capsule-alone trajectory ($D_r/D_o = 1$).

Temperatures were obtained from the heating rate data of Figures 17 and 18 by substitution into the relation

$$T = \{K_1 \dot{q}/\varepsilon\nu\}^{1/4}$$

Figures 19 and 20, respectively, show the results for the nonlifting and lifting re-entries. For computing the temperatures, a value of $\varepsilon = 0.8$ was used. The parameter K_1 is a heating-rate multiplication factor which takes into account the blade curvature and the increase in heating rate caused by the capsule's bow shock wave. A value of $K_1 = 2.85$ was obtained analytically, and later experimental results [Ref. 13] indicate that this estimate is slightly optimistic, and the value should be higher, about 3.3, except at shock impingement. This 15% increase in K_1 would increase the temperatures shown herein by about 4%. For the nonlifting re-entry a diameter ratio of nearly 4 is required for the temperature limit used. For the lifting re-entry the diameter ratio required would generally have to be larger than 10.

The indication that the lifting re-entry would produce excessive temperatures led to the notion of delaying the lifting phase until sometime after peak heating. An additional study was made, therefore, to determine the effect of delayed deployment on range performance.

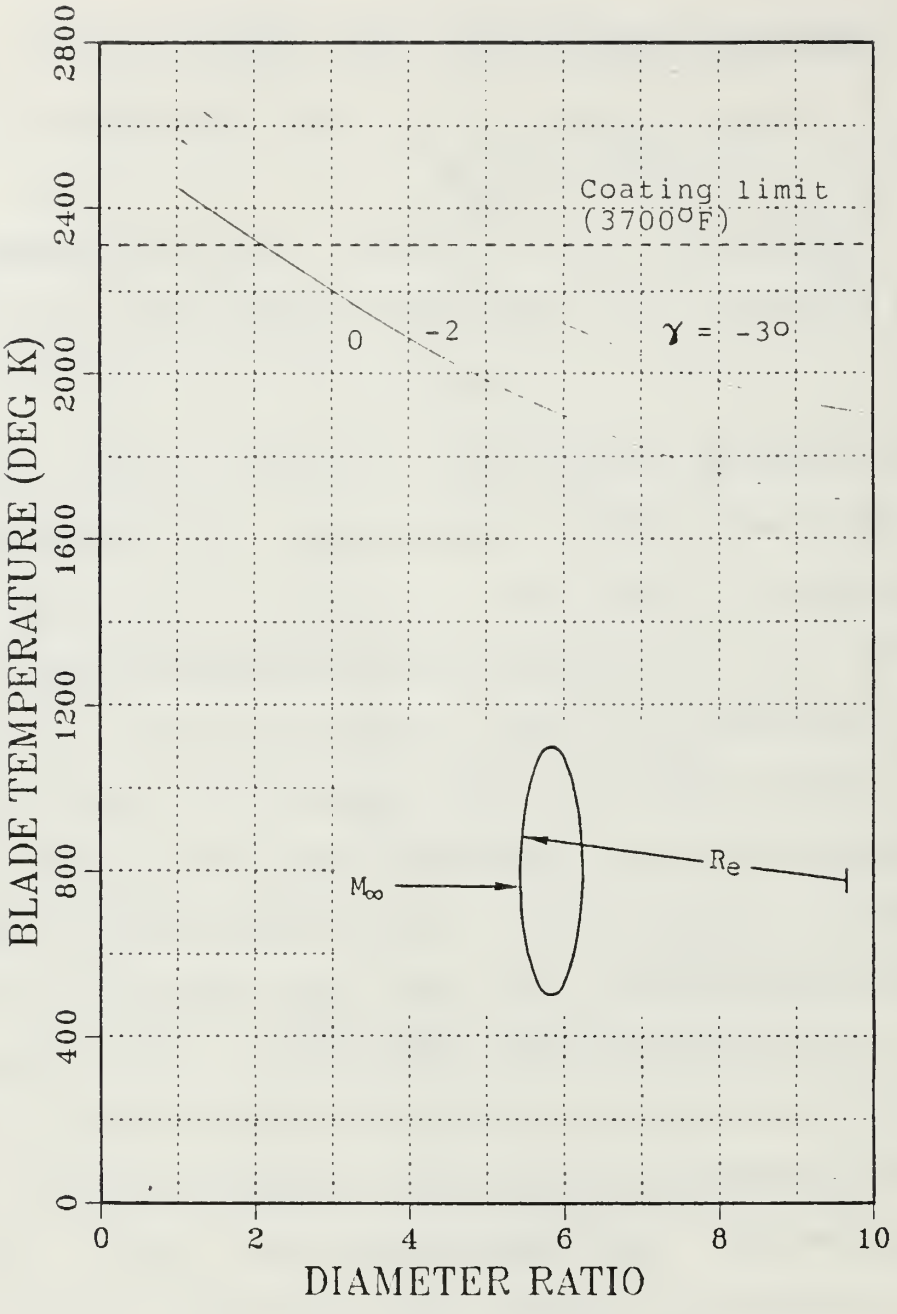

Figure 19

Diameter Ratio vs. Maximum Blade Temperature
(Nonlifting; R_e = 1.524 m)

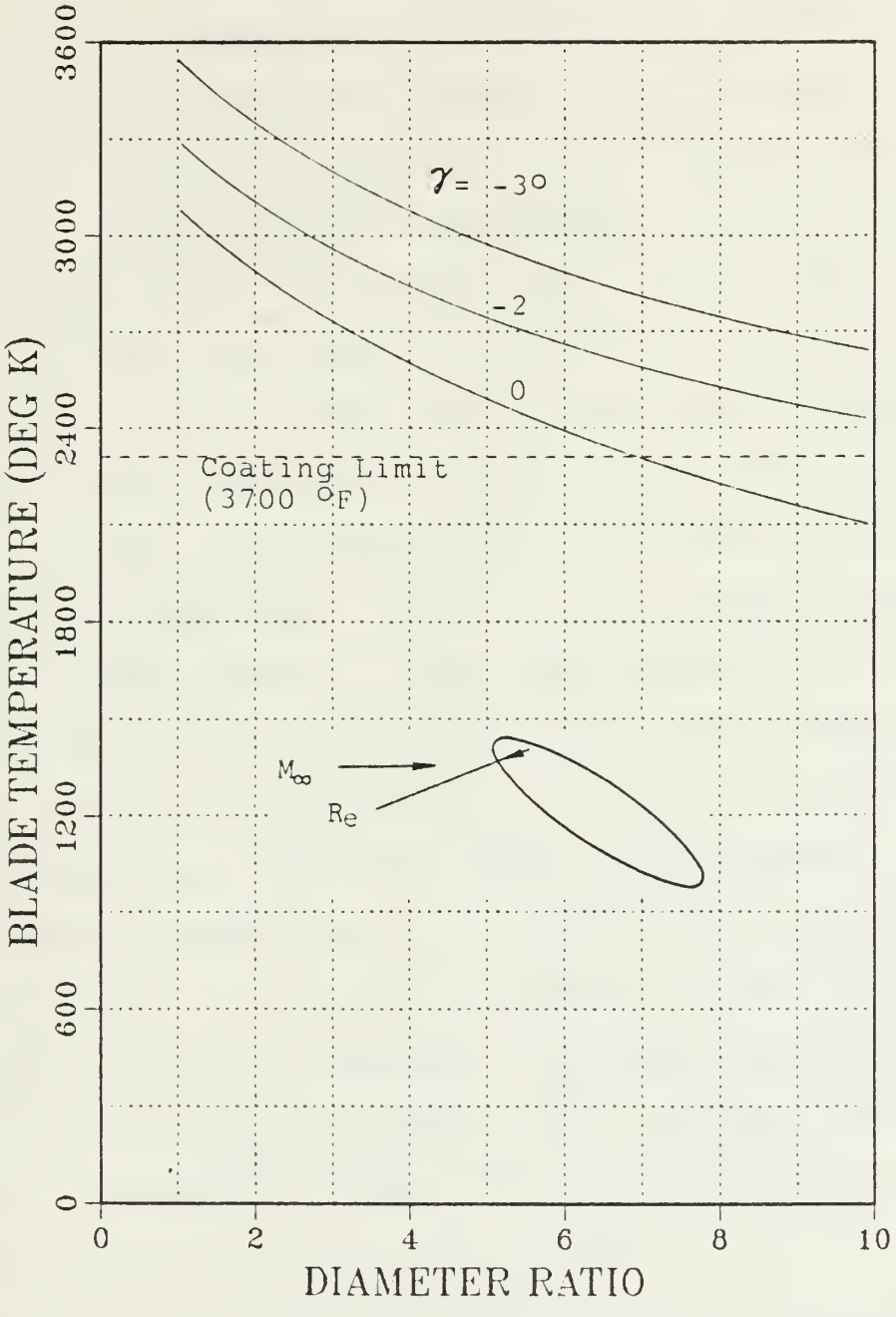

Figure 20

Diameter Ratio vs. Maximum Blade Temperature
(Lifting; R_e = 1.524 m)

6. Effects of Delayed Rotor Deployment

The effect of delayed rotor deployment on lateral range was investigated for configurations having a D_r/D_o of 2 and 4. Figures 21 and 22 show the results.

Both lifting and nonlifting modes of capsule operation prior to rotor deployment were investigated, and the assumption was made that the vehicle could be banked in the lifting mode prior to rotor deployment. Not being able to utilize the capsule lift resulted in the loss of a substantial portion of the lateral range capability.

The percentage reduction in lateral range resulting from delayed rotor deployment is greater for the $D_r/D_o = 4$ vehicle than for the $D_r/D_o = 2$ vehicle because the diameter ratio 4 vehicle has a higher L/D, which cannot be utilized until the rotor is deployed. For both diameter ratios, the L/D prior to rotor deployment was the same. Figure 23 shows the longitudinal range as a function of rotor deployment Mach number for $D_r/D_o = 2$. Curves are shown for both modes of capsule operation prior to rotor deployment. Without being able to use capsule lift prior to rotor deployment, the reduction in longitudinal range is considerable even for deployment at a Mach number of 18.

Deploying the rotor at various Mach numbers along the trajectory implies deployment at various heating rate levels. If rotor deployment is made at Mach numbers exceeding about 17 for a diameter ratio of 4, the blades

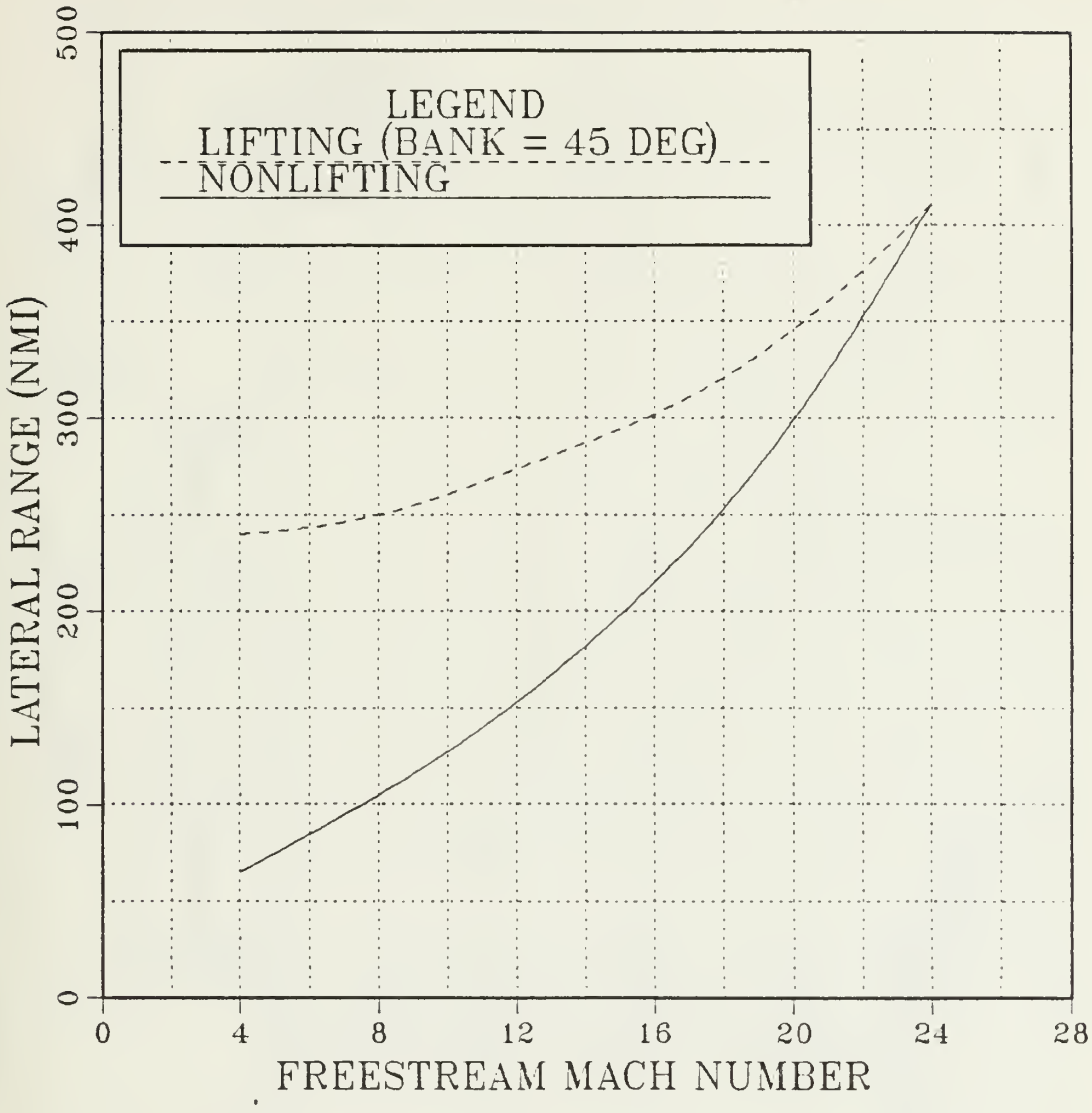

Figure 21

Lateral Range vs. Deployment Mach Number

(γ = -3^0; D_r/D_c = 2)

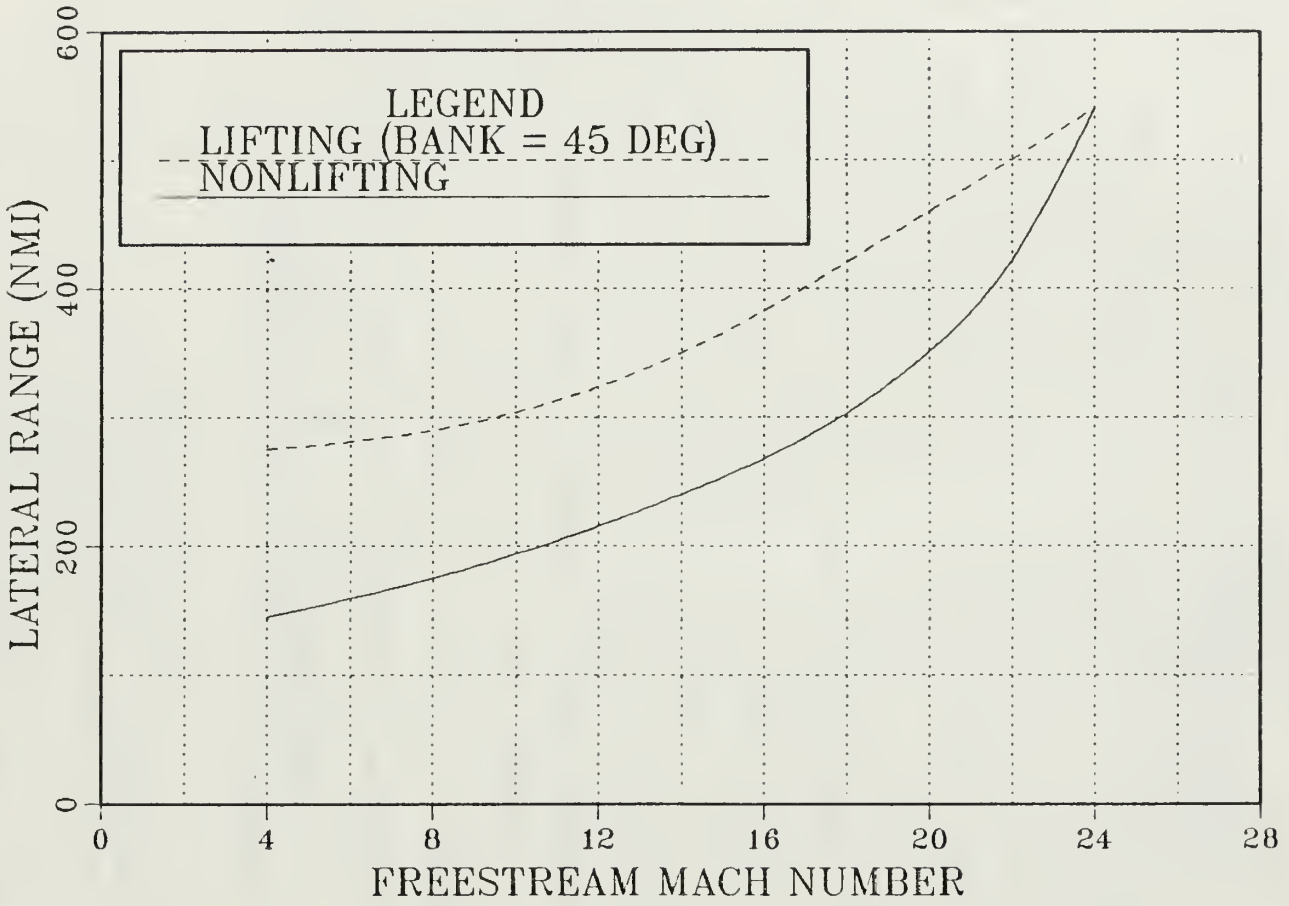

Figure 22

Lateral Range vs. Deployment Mach Number
($\gamma = -3^0$; $D_r/D_c = 4$)

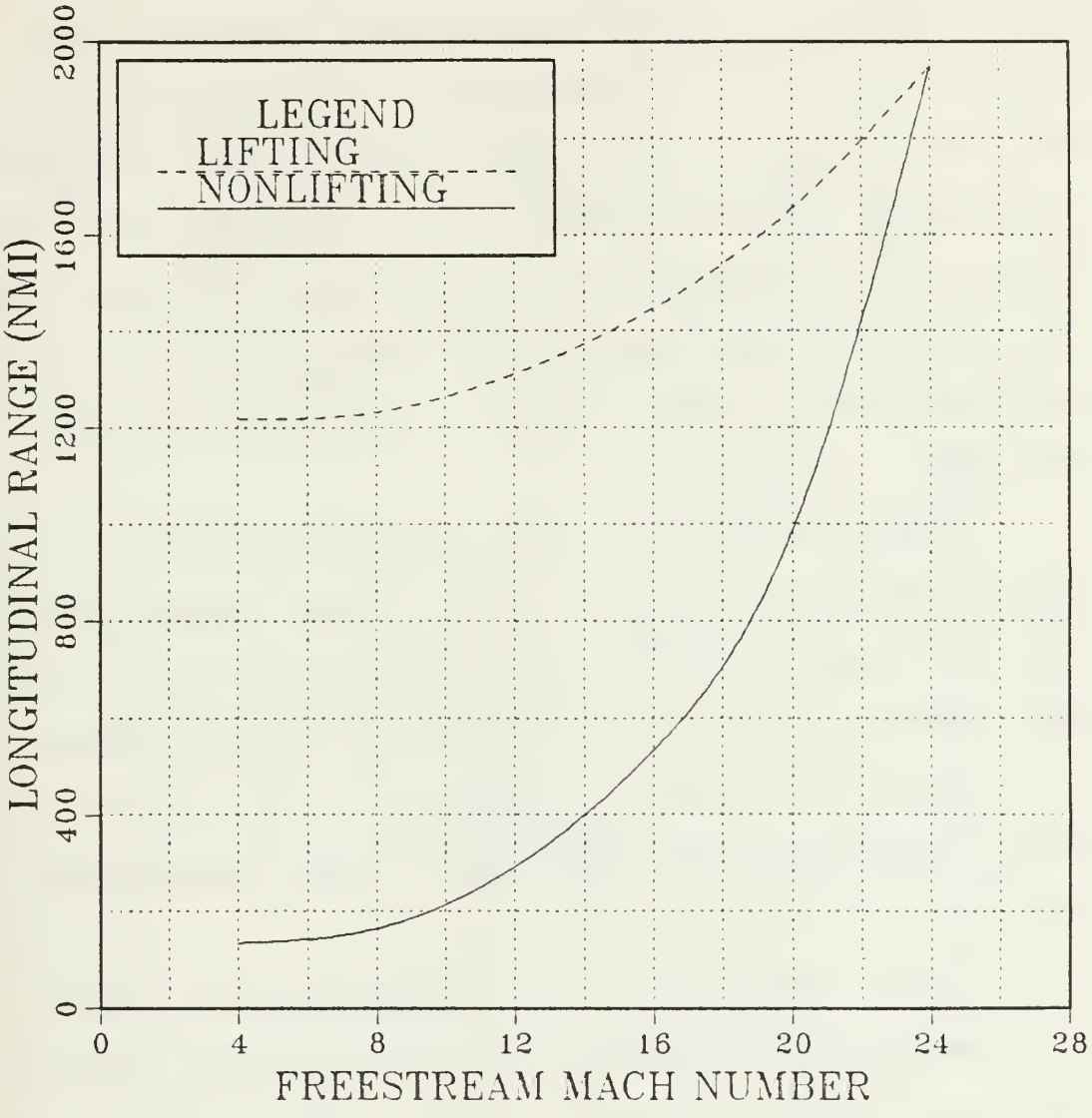

Figure 23

Longitudinal Range vs. Deployment Mach Number
(γ = -3^0; D_r/D_c = 2)

would possibly require an ablative coating for heat protection. This is thought to be impractical because of the high probability of nonuniform ablation causing an intolerable vibration level. At deployment Mach numbers above 8, and less than 17, a coated blade structure similar to the type discussed earlier is appropriate. At rotor deployment Mach numbers below 8, no heat protection is required.

Figure 24 shows the radiation equilibrium rotor blade temperature as a function of Mach number for a rotor re-entry vehicle of $D_r/D_c = 4$ re-entering at -2°. With a stabilized zirconium oxide coating having a temperature limit of 2320 $^{\circ}$K (3700 $^{\circ}$F), operation of the rotor in the lifting mode must be delayed until a Mach number near 17 is reached.

The results of this investigation led to the development of the sequence of operating modes illustrated in Figure 25 for the rotor re-entry vehicle. At re-entry, the rotor is deployed and the vehicle flown in a near-axial attitude with the rotor coned back 45° to avoid capsule bow shock impingement (as indicated by the heat-transfer results of Reference 13). Within this constraint, an L/D of nearly 0.3 is possible. At a Mach number of about 16, transition begins to the glide flight (autogyro) attitude and should be completed by the time a Mach number of 4 is reached. From this point to subsonic velocities, supersonic glide flight

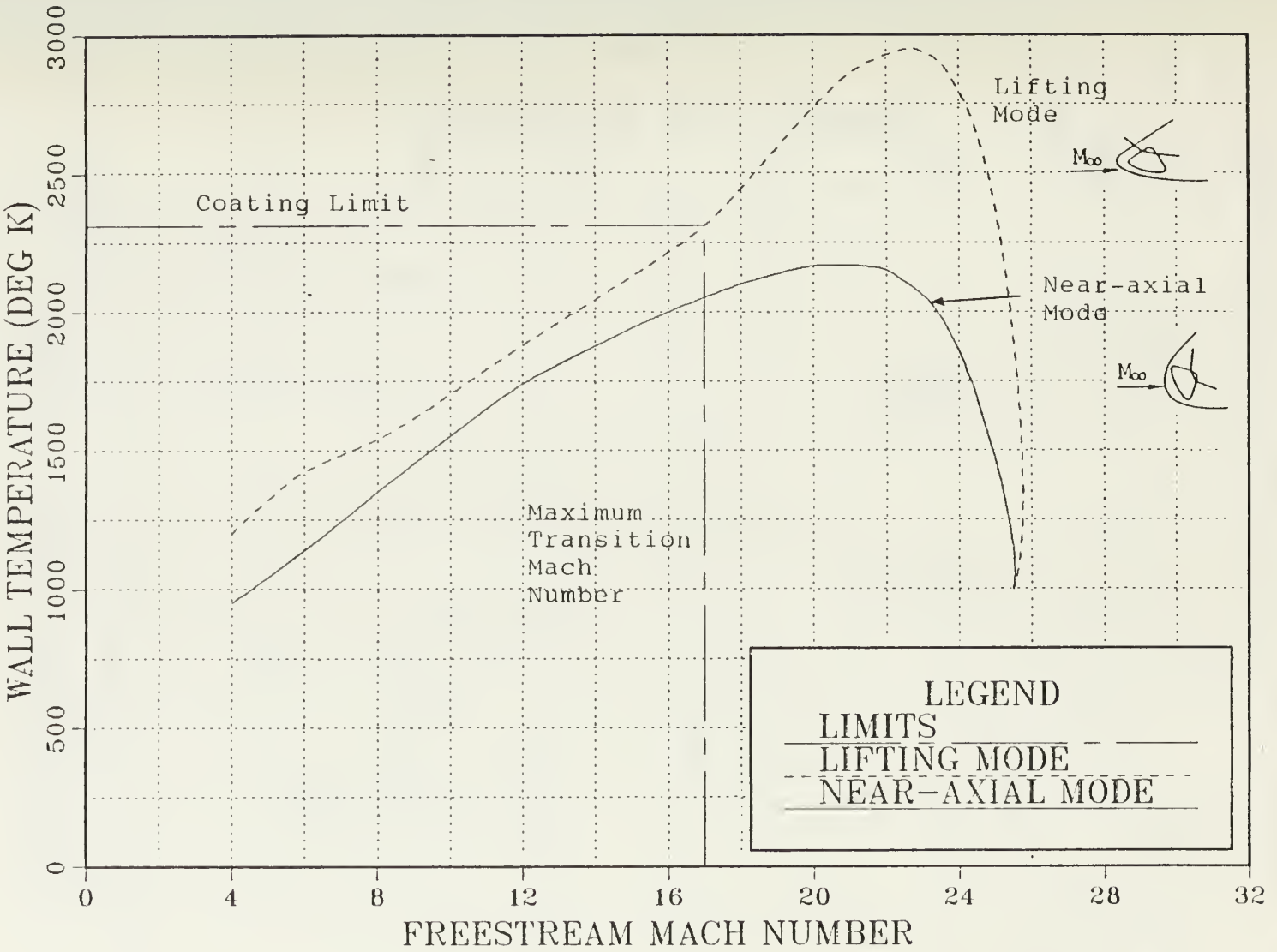

Figure 24

Stagnation-point Wall Temperature vs. Mach Number

($\gamma = -2^{0}$; $D_r/D_c = 4$)

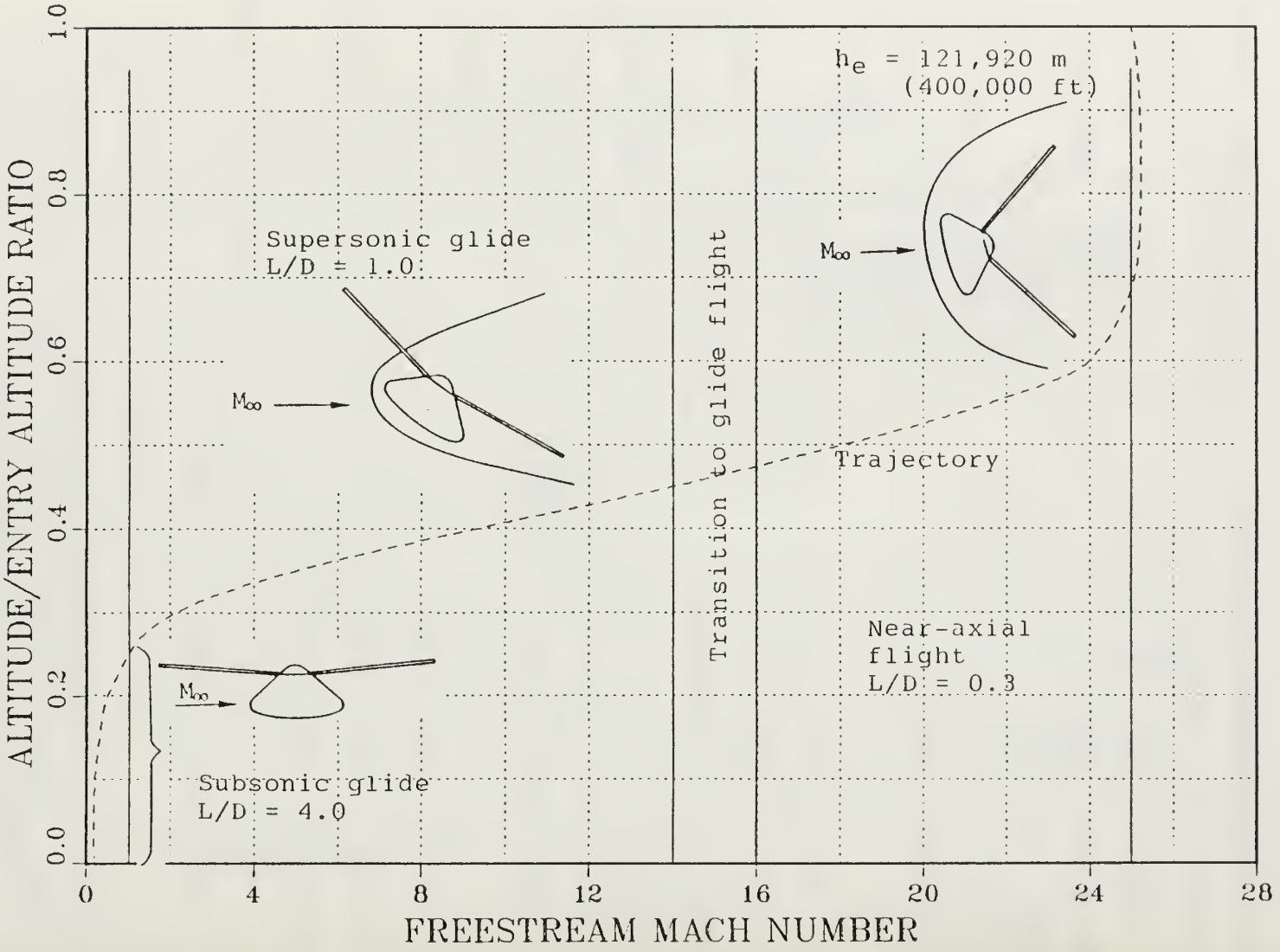

Figure 25

Rotor Vehicle Operating Modes

is maintained at an L/D near 1.Ø. The subsonic flight portion will be in the L/D = 4.Ø range. The vehicle then lands like a helicopter with the power off. This sequence of operating modes has not taken into account any potential problems of vehicle trim at the flight attitudes indicated.

IV. CONCLUSIONS

The results of this theoretical examination of the rotor aerodynamic characteristics and performance of a rotor re-entry vehicle have led to the following conclusions:

1. The rotor has a stable operating range at low negative blade pitch angles, which was not apparent from low-speed helicopter operation.

2. In axial flight, the rate of increase of rpm with small blade pitch angle changes is quite severe and will require precise control of blade pitch to prevent overspeeding.

3. In axial flight attitudes, there is good agreement between theoretical and experimental rotor drag at least for subsonic and supersonic speeds.

4. When used throughout the entire re-entry trajectory in the glide mode, the rotor added to the capsule results in substantial gains in lateral range.

5. On the basis of gains in maximum range and magnitude of the maximum decelerations, the most optimum rotor-to-capsule diameter ratio is about 4.

6. From a heating standpoint, the vehicle cannot be used in the glide mode throughout the entire re-entry trajectory and maintain the temperature constraint of 2320 ^{o}K (3700 ^{o}F) on the rotor blade coating.

7. Since bow shock impingement on the rotor blades can cause heating rates eight times that of the capsule stagnation value, the rotor may have to be coned back during the peak heating portion of the re-entry trajectory, thus reducing available rotor thrust.

8. Delaying rotor deployment causes large reductions in the maximum lateral range capability; however, if capsule lift can be utilized prior to rotor deployment, the loss in lateral range is decreased.

V. RECOMMENDATIONS

A. GENERAL

This theoretical examination was intended to be an initial investigation into the problem of using a re-entry vehicle incorporating an autorotating rotor to improve lateral range capability and provide much lower landing speeds, thus increasing safety in re-entry operations and providing greater operational utility. To simplify calculations, a rotor-plus-capsule configuration was studied; however, the ultimate design would combine the rotor system with a lifting body shape such as the NASA M-2 or HL-10 or perhaps a design similar to the Space Shuttle delta-wing. Reference 14 discusses an example of this type of combination, shown in Figure 26; however, the discussion limits the use of the rotor to the approach and landing phases of recovery. The next step, similar to the objective of this study, would be to determine the aerodynamic and performance characteristics of that type of combination while using the rotor system during the entire re-entry trajectory.

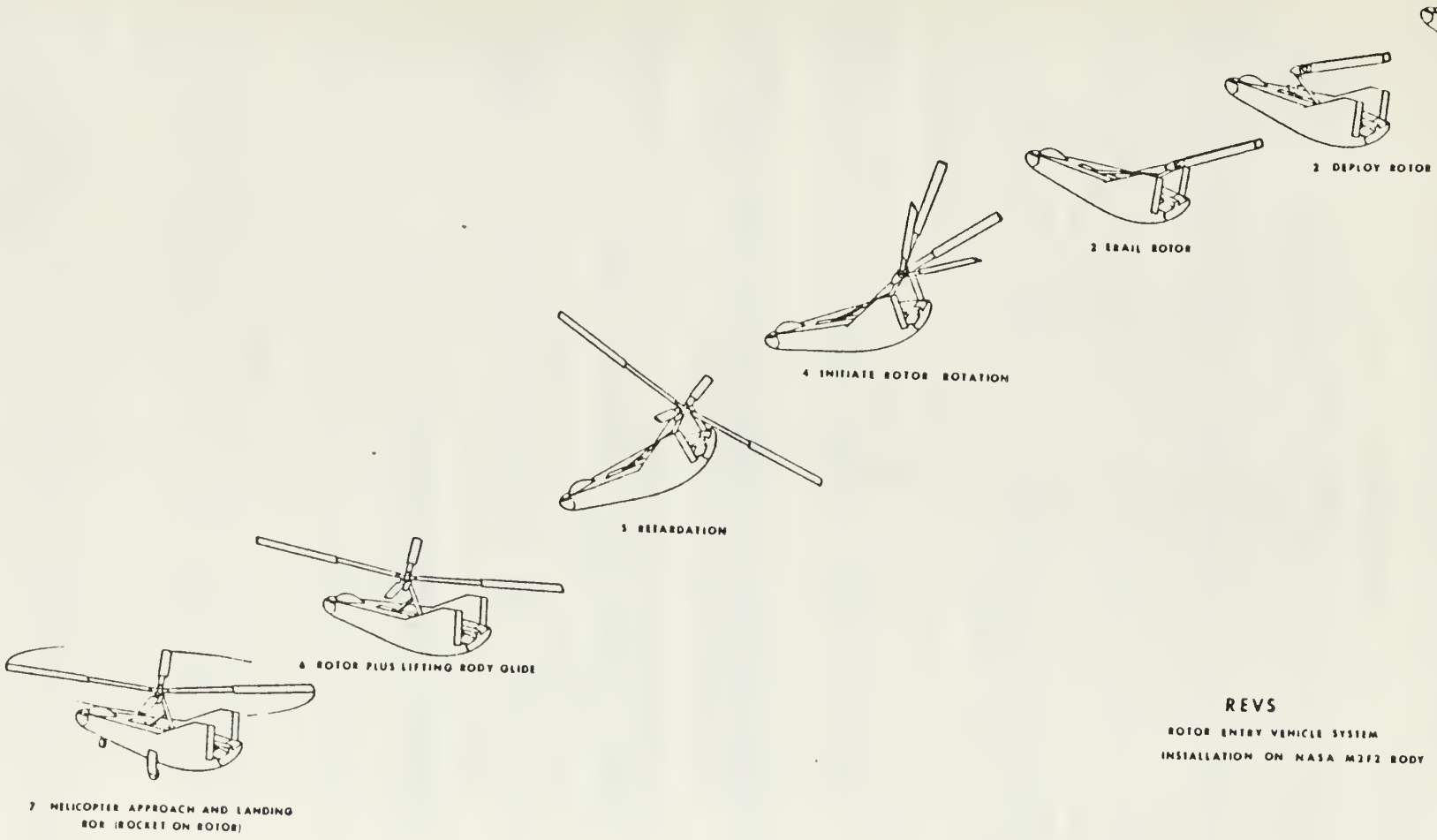

Figure 26

Rotor Entry Vehicle System
[Source: Ref. 14]

B. SPECIFIC

The following specific recommendations are included for consideration:

1. This study should be expanded to include designs combining a rotor and lifting body shape.

2. Research should be conducted to find alternative rotor structural materials having a higher operating temperature limit than the one used for this study. A higher limit would permit earlier rotor deployment, thereby realizing increased performance gains.

3. Prior to actual production of a vehicle, much experimental work remains to be done, and the following list of items (by no means complete) should be considered:

   * predictions of rotor weight, size, and cost

   * development of a complete control system, manual and/or automatic, which includes attitude trim capability

   * modification of the navigation system to fully take advantage of the improved performance provided by the rotor system

   * investigation of other blade deployment schemes such as flexible, inflatable blades

   * consideration of power augmentation of the rotor by tip jets or other means in order to reduce rotor size and weight and/or extend the range capabilities or provide a short period of hover

   * appropriate crew training.

LIST OF REFERENCES

1. Kretz, M.: *Application of Rotary Wing Techniques to Atmospheric Re-entry and Launch Vehicle Recovery Problems.* Paper presented at the European Symposium on Space Technology, London, England, June 1961.

2. Hodson, J.S.: *Low Speed Wind Tunnel Test of 12-foot and 14-foot Diameter Rotochutes.* Kaman Aircraft Corporation Report T-93, January 1957.

3. Barzda, J.J.: *Test Results of Rotary-Wing Deceleration Feasibility Studies for Capsule Recovery Applications.* Society of Automotive Engineers (SAE) Paper No. 756D, September 1963.

4. Haig, C.R., Jr.: *The Use of Rotors for the Landing and Reentry Braking of Manned Spacecraft.* International Aerospace Society Paper 60-17, 1960.

5. Galigher, L.L.: *Wind Tunnel Tests of the Kaman KRC-6M Rotochute at Supersonic Speeds.* Arnold Engineering Development Center AEDC-TDR-63-128, July 1963.

6. Robinson, D.W., et al.: *Investigation of Stored Energy Rotors for Recovery.* Kaman Aircraft Corporation, Aeronautical Systems Division TDR-63-745, December 1963.

7. Barzda, J.J.: "Rotors for Recovery", *Journal of Spacecraft and Rockets,* Vol. 3, No. 1, pp. 104-109, January 1967.

8. Love, E.S.: "Reentry Vehicles: General Concepts, Operational Modes, and Performance Characteristics", *Proceedings of the Conference on Physics of the Solar System and Reentry Dynamics*, Virginia Polytechnic Institute, Blackburg, VA, July 31 to August 11, 1961.

9. Clark, E.L. and Trimmer, L.L.: *Equations and Charts for the Evaluation of the Aerodynamic Characteristics of Re-entry Configurations by the Newtonian Theory*, Arnold Engineering Development Center, AEDC-TDR-74-25, March 1974.

10. Ham, N.D.: "An Experimental and Theoretical Investigation of a Supersonic Rotating Decelerator", *Journal of the American Helicopter Society,* pp. 8-18, January 1963.

11. Haig, C.R., Jr.: *Aerodynamic Analysis of a Rotor in a Fully Stalled Propeller Braking State.* Bell Helicopter Report 8008-099-003, March 1960.

12. Haig, C.R., Jr.: *An Aerodynamic Analysis of a Lifting Rotor in Hypersonic Flight.* Bell Helicopter Report 8008-099-001, June 1959.

13. Smith, R.C. and Levin, A.D.: *Heat-Transfer Measurements on the Rotor Blade of a Rotor Entry Vehicle Model.* NASA TN D-4065, 1967.

14. Hollrock, R.H. and Barzda, J.J.: *Rotor Entry Vehicle Systems (REVS) for Safe Landings.* Paper No. 67-203 presented at the American Institute of Aeronautics and Astronautics 5th Aerospace Sciences Meeting, New York, January 23-26, 1967.

INITIAL DISTRIBUTION LIST

		No. Copies
1.	Defense Technical Information Center Cameron Station Alexandria, VA 22304-6145	2
2.	Library, Code 0142 Naval Postgraduate School Monterey, CA 93943-5002	2
3.	LCDR Robert G. Struth, Jr., USN Pacific Missile Test Center Code 100D NAS Pt. Mugu, CA 93042	3

271
18070 2

DUDLEY KNOX LIBRARY
NAVAL POSTGRADUATE SCHOOL
MONTEREY, CALIFORNIA 93943-5002

221172

Thesis
S85654 Struth
c.1 A theoretical examination of a re-entry capsule incorporating an autorotating rotor.

221172

Thesis
S85654 Struth
c.1 A theoretical examination of a re-entry capsule incorporating an autorotating rotor.

A theoretical examination of a re-entry

3 2768 000 76089 6
DUDLEY KNOX LIBRARY